Title:

Morphogenetic forces planar polarize LGN/Pins in the embryonic head during *Drosophila* gastrulation

Authors: Jaclyn Camuglia[1], Soline Chanet[2], Adam C Martin[1, 3]

---

[1] Biology Department, Massachusetts Institute of Technology, 77 Massachusetts Ave., Cambridge, MA 02139

[2] Center for Interdisciplinary Research in Biology, Collège de France, 11 Pl. Marcelin Berthelot, 75231 Paris

[3] Corresponding author: acmartin@mit.edu

Abstract:

Spindle orientation is often achieved by a complex of Pins/LGN, Mud/NuMa, Gαi, and Dynein, which interacts with astral microtubules to rotate the spindle. Cortical Pins/LGN recruitment serves as a critical step in this process. Here, we identify Pins-mediated planar cell polarized divisions in several of the mitotic domains of the early *Drosophila* embryo. We found that neither planar cell polarity pathways nor planar polarized myosin localization determined division orientation; instead, our findings strongly suggest that Pins planar polarity and force generated from mesoderm invagination are important. Disrupting Pins polarity via overexpression of a myristoylated version of Pins caused randomized division angles. We found that disrupting forces through chemical inhibitors, depletion of an adherens junction protein or blocking mesoderm invagination disrupted Pins planar polarity and spindle orientation. Furthermore, directional ablations that separated mesoderm from mitotic domains disrupted spindle orientation, suggesting that forces transmitted from mesoderm to mitotic domains can polarize Pins and orient division during gastrulation. To our knowledge, this is the first *in vivo* example where mechanical force has been shown to polarize Pins to mediate division orientation.

39 **Introduction:**

40

41 Epithelial morphogenesis and homeostasis are influenced by cell division orientation, which can
42 occur along specific axes relative to both the epithelial plane and the polarity of an organ/organism
43 (Baena–Lopez et al., 2005; Kulukian and Fuchs, 2013; Lancaster and Knoblich, 2012; Morin and
44 Bellaiche, 2011). Epithelia are tissues composed of cells that are organized in a sheet and held
45 together by junctions, which maintain the integrity of the tissue as well as the apical-basal polarity
46 of cells (Choi et al., 2013; Classen et al., 2005; Cox et al., 1996; Gumbiner, 2005; Harris and
47 Peifer 2005; Tepass, 1997; Wang and Margolis, 2007). In epithelia, asymmetric cell divisions, in
48 which cellular components are distributed unequally to daughter cells, result in one daughter cell
49 leaving the epithelium. In contrast, symmetric divisions in epithelia divide cellular components
50 equally, and usually results in both daughter cells remaining in the tissue. Orientation of the mitotic
51 spindle is what determines whether a division is symmetric or not, as spindle orientation
52 determines division orientation (Cabernard and Doe, 2009; Gonczy and Rose, 2005; Lechler and
53 Fuchs, 2005; Mao et al., 2011; Nakajima et al., 2013). In addition, the spindle orientation with
54 respect to organ/organism axis can promote directional growth and/or stress dissipation in tissues
55 (Campinho et al., 2013; Legoff et al., 2013; Mao et al., 2011; Mao et al., 2013; Wyatt et al., 2015).
56 Spindle orientation is often achieved by a complex of Partner of Inscuteable (Pins)/LGN,
57 Mushroom Body Defect (Mud)/Nuclear Mitotic Apparatus (NuMa), Gαi, and Dynein. In this
58 complex, Pins/LGN acts as a linker between Gαi and Mud, which is also bound to a Dynein-
59 Dynactin complex. Dynein's motor activity provides the force to rotate the spindle (Bergstralh et
60 al., 2013; Busson et al., 1998; Fielmich et al., 2018; Grill and Hyman, 2005; Johnston et al., 2009;
61 Nguyen-Ngoc et al., 2007; Siller and Doe, 2008). In *Drosophila* neuroblasts, asymmetric division
62 and spindle orientation is dependent on Pins/LGN recruitment to the apical cortex. Apical proteins
63 recruit Inscuteable (Insc), which in turn recruits Pins/LGN and the spindle rotation complex. Pins

64 null mutants exhibit defects in spindle orientation in neuroblasts (Cabernard and Doe, 2009;
65 Schaefer et al., 2000; Siller et al., 2006; Yu et al., 2006). In symmetric epithelial cell divisions,
66 spindle orientation also depends on Pins, which is recruited to the lateral cortex by the lateral
67 domain protein, Discs large (Dlg). Loss of Pins, Dlg, or disrupted recruitment of Pins by Dlg causes
68 aberrant asymmetric cell divisions in epithelia and cell loss (Bell et al., 2015; Bergstralh et al.,
69 2013; Carvalho et al., 2015). Furthermore, in planar cell polarized divisions of the sensory organ
70 precursor cells in the *Drosophila* dorsal thorax, asymmetric determinant segregation and spindle
71 orientation depend on planar polarized Pins and E-cadherin localization, respectively (Bellaïche
72 et al., 2001; Le Borgne et al., 2002).

73 In addition to molecular cues, mechanical cues also orient cell division. For example, in
74 isolated cell cultures, cell division orientation has been shown to directly respond to stress by
75 aligning with applied forces (Fink et al., 2011; Matsumura et al., 2016; Thery et al., 2007; Thery
76 et al., 2005). Cells also respond to force through its influence on cell shape. The connection
77 between cell shape and division axis is known as the long axis rule or Hertwig's rule and was first
78 observed over 100 years ago (Hertwig, 1884). However, the mechanisms through which force,
79 cell shape, and molecular cues are interconnected to influence cell division remain an active area
80 of research. In epithelial tissues, cell division/spindle orientation occurs along the tension axis,
81 which can dissipate tension and influence cell packing (Campinho et al., 2013; Gibson et al.,
82 2011; Godard et al., 2020; Mao et al., 2011; Scarpa et al., 2018; Wyatt et al., 2015). In the
83 *Drosophila* pupal notum and *Xenopus,* cell shape has been shown to affect the spindle angle
84 through the influence of molecular cues localized at tri-cellular junctions, which provide a 'memory'
85 for interphase cell shape (Bosveld et al., 2016; Nestor-Bergmann et al., 2019). In contrast, in the
86 *Drosophila* oocyte, follicular epithelium, and parasegmental boundaries and cultured MDCK cells,
87 molecular cues, like Pins/LGN and Mud/NUMA, do not localize to tri-cellular junctions, implying
88 that cells use additional strategies to promote force-oriented spindle rotation, in some contexts
89 (Finegan et al., 2019; Gloerich et al., 2017; Scarpa et al., 2018; Yu et al., 2006). For example,

90 mechanical cues have been shown to recruit the Pins/LGN machinery to adherens junctions in
91 MDCK cells (Hart et al., 2017). Mitotic rounding forces have also been shown to be important for
92 proper spindle orientation and morphology (Chanet et al., 2017; Kunda et al., 2012). The
93 combinatorial action of mechanical and molecular cues used to orient spindles is incompletely
94 understood. Here, we use the *Drosophila* embryo as a powerful model organism that is uniquely
95 tractable - exhibiting mirror symmetric domains that undergo highly stereotyped oriented divisions
96 - to uncover the relationship between mechanical and molecular cues that coordinate division
97 orientation and morphogenetic movements in an embryo.

98 During development, the early *Drosophila* embryo undergoes thirteen cycles of
99 synchronous nuclear divisions with no intervening gap phases. After these thirteen cycles of
100 nuclear division, embryonic cells arrest in G2. Cycle 14 divisions occur in a highly stereotyped
101 pattern defined by *string* (*Drosophila* Cdc25 homologue) expression in pockets of cells across the
102 embryo. These pockets of cells that divide together are termed mitotic domains (Edgar and
103 O'Farrell, 1989; Foe, 1989). Some of these domains have been observed to have oriented
104 divisions, but the mechanism underlying division orientation is unknown (da Silva and Vincent,
105 2007; Hartenstein and Campos-Ortega, 1985; Hartenstein et al., 1987; Stern et al., 2022; Wang
106 et al., 2017). We found that spindle orientation is a dynamic process in which spindles are not
107 assembled in position, but rather rotate to achieve orientation in mitotic domains 1, 3, and 5 (MDs
108 1, 3, and 5) in the dorsal 'head' and are oriented in the direction of eventual tissue
109 movement/elongation. We discovered that these oriented symmetric divisions and those of MD
110 14, which had previously been shown to exhibit force dependent oriented symmetric divisions
111 (Wang et al., 2017), require planar polarized Pins.
112
113
114
115

116 **Results:**

117

118 *Early mitotic domains in the Drosophila head exhibit spindle rotation and planar polarized division.*

119 Located on the dorsal side of the *Drosophila* embryo 'head', MD 1, 3, and 5 undergo
120 division during gastrulation, 200 minutes after egg deposition (AED). MD3 is the anterior most
121 mitotic domain and comprises around thirty cells, MD1 is the next most anterior domain and
122 consists of two mirrored clusters of around 40 cells, and MD5 is located just anterior to the
123 cephalic furrow and consists of two mirrored clusters containing around 30 cells (Figure 1A, B).

124 We initially visualized division axis in embryos expressing fluorescently-tagged non-
125 muscle myosin II to mark cytokinetic rings and fluorescently tagged myristoylation sequence of
126 Gap43 to mark cell membranes. Cytokinetic rings form perpendicular to the division axis. In MDs
127 1, 3, and 5, cytokinetic rings are oriented roughly perpendicular to the AP axis. (Figure 1C). To
128 further visualize the division process and assess dynamics during division, we used embryos
129 expressing fluorescently-tagged CLIP170 to mark the mitotic spindle (Figure 1D, Figure 1- video
130 1). For this paper, we will display all head images with the anterior pole towards the top. To
131 quantify the alignment of the divisions with the AP axis, we measured the angle between the
132 spindle and the AP axis, where an angle of 0 indicates perfect alignment with the AP axis and an
133 angle of 90 indicates alignment with the dorsal-ventral (DV) axis (Figure 1E). Spindles were
134 measured after anaphase, when spindle position becomes fixed. MDs 1, 3, and 5 divisions occur
135 almost entirely within 30° of the AP axis (Figure 1F-H). Markedly in MD1, the majority of spindles
136 were slightly tilted relative to the AP axis and mirror symmetric, such that spindles on the left side
137 divided within 0 to 30° of the AP axis (Figure 1C and I) and spindles on the right side divided
138 within 0 to -30° of the AP axis (Figure 1D and J).

139 Notably, we found that mitotic spindles are not initially oriented with the AP axis and form
140 with no preferential orientation. Spindles then rotated up to 90° to achieve a final orientation

141 (Figure 1D). Despite dividing with a mirror-symmetric tilt away from the AP axis, we observed no
142 chirality in spindle rotation; on the left side of MD1 53% of measured spindles rotated
143 counterclockwise and 47% rotated clockwise, on the right side 46% rotated counterclockwise and
144 54% clockwise. Together these data show that MDs 1, 3, and 5 exhibited oriented divisions and
145 this orientation is achieved by spindle rotation toward an angle ~ 30° from the AP axis. We next
146 asked what cue(s) could coordinate the spindle rotation and division orientation.
147
148 *Planar polarized divisions require polarized Pins localization*
149 Because spindles exhibited a pronounced rotation after assembly, we examined
150 components of the spindle rotation machinery, Pins and Mud. We discovered that MDs 1, 3, and
151 5 all exhibit planar cell polarity of Pins. The Pins planar cell polarity is dependent on cell cycle
152 state: mitotic cells exhibit planar polarized Pins, whereas Pins is uniformly distributed along lateral
153 membranes of interphase cells (Figure 2A, Figure 2- video 1). We quantified Pins polarization by
154 modifying previously described polarization quantifications of mitotic cells (Besson et al., 2015).
155 We used embryos expressing fluorescently labelled Pins and fluorescent membrane marker
156 Gap43::mCherry, and measured the intensity of Pins::YFP and Gap43::mCherry around the
157 membrane. We found that in MD1, the Pins intensity is highest on the posterior side of the cells
158 and the crescent of Pins intensity peaks just past the posterior-most point of the cell cortex (Figure
159 2C and C'). The ratio of the point of greatest Pins intensity to the average of the two adjacent
160 troughs averaged over 3 embryos, was significantly greater than the same ratio calculated from
161 the Gap43::mCherry signal (peak-to-trough ratio Pins, 1.39±0.1017 and Gap43::mCherry,
162 1.04±0.0406, mean and S.D., p=1.7057e-08), demonstrating that this polarity was not caused by
163 membrane inhomogeneity. Gap43::mCherry also had a more uniform labeling along the
164 membrane in MD cells (Figure 2B, D, and D'). Though our imaging resolution is not sufficient to
165 determine whether Pins is localized solely on the posterior side of MD1 cells or both the posterior
166 and anterior sides when groups of cells round up together, we find that cells on the boundary of

167 MD1 display Pins crescents enriched on the posterior side. Interestingly, from observation of
168 boundary cells, we find Pins was enriched on the posterior side of MDs 1 and 3, but the anterior
169 side of MD5 (Figure 2- figure supplement 1).

170 To ensure Pins polarization was not a consequence of expressing non-endogenous levels
171 of Pins, we fixed and stained embryos to localize endogenous Pins. We found that similar to
172 Pins::YFP, endogenous Pins was planar polarized in mitotic MD 1 cells (Figure 2E-F). We also
173 looked at components of the spindle rotation machinery complex downstream of Pins, namely
174 Mud. It appears that Mud follows a similar localization pattern as Pins and is polarized in crescents
175 in mitotic cells of MD1, although Mud also strongly labels spindle poles (Figure 2G). Based on
176 our live and fixed imaging, we conclude that MDs 1, 3, and 5 cells exhibit planar polarized Pins
177 localization during mitosis.

178 In addition to MDs 1, 3, and 5 we examined MD14, which has previously been shown to
179 exhibit force dependent planar polarized divisions (Wang et al., 2017). Mitotic cells within MD14
180 exhibited planar polarized Pins, similar to what we saw for MD 1 (Figure 2H). Posterior crescents
181 of Pins form in the mitotic cells of MD 14, though the crescent is broader than in MDs 1, 3, and 5.
182 The peak to trough ratio for Pins in MD14 was significantly different from control Gap43::mCherry
183 (1.22±0.0914 and 1.04±0.1115, respectively, mean and S.D., p=3.1726e-06) (Figure 2H-K').
184 Thus, MD14 cells also exhibit planar polarized Pins localization.

185 We next sought to establish whether there was a connection between Pins polarity and
186 spindle orientation. Using embryos expressing fluorescently-tagged tubulin and fluorescently-
187 tagged Pins we monitored the timing of Pins polarization and spindle rotation. We found that Pins
188 polarization preceded spindle rotation and is abolished shortly after anaphase, when the spindle
189 position is finalized (Figure 3A-B, Figure 3- video 1). The correlated timing between Pins
190 polarization and spindle rotation suggests Pins is responsible for the spindle achieving its
191 polarized orientation. To determine the relationship between Pins polarity and spindle rotation we
192 compared the angle of maximum Pins intensity to the division angle. We found that there was a

193 strong correlation between angular position of maximum Pins intensity and the anaphase spindle
194 angle in MD 1 (Figure 3C). Previous studies have shown division orientation often follows the long
195 axis of the interphase cell shape (Hertwig, 1884; Minc et al., 2011; Tsou et al., 2003). To
196 determine whether division angle in the MD1 could also be related to cell shape, we compared
197 the interphase cell long-axis angle to the division angle. In contrast to Pins polarity, there was no
198 correlation between interphase cell shape and division angle, indicating the divisions of MD1 do
199 not follow the long axis rule (Figure 3- figure supplement 1). Together these data show that
200 division orientation correlates with Pins localization, but not interphase cell shape. We also
201 analyzed Pins and tubulin within MD14, which is located at the ventral midline (Figure 3D). Similar
202 to MD 1, Pins polarization preceded spindle rotation (Figure 3E-F).

203 To test the functional requirement of Pins polarity, we analyzed spindle orientation in
204 embryos overexpressing a myristoylated Pins. Myristoylation covalently attaches a myristoyl
205 group to a protein so the protein associates with the plasma membrane in an unregulated manner.
206 Overexpression of myristoylated Pins, but not wild-type Pins, caused Pins to be uniformly
207 distributed along the membrane during mitosis and abolished Pins planar polarity (Figure 3- figure
208 supplement 2). Importantly, perturbation using myr-Pins did not obviously disrupt other
209 morphogenetic events during gastrulation. Mesoderm invagination, cephalic furrow invagination,
210 and germ band extension all occur in embryos expressing myr-Pins. Further, expression of myr-
211 Pins does not impact the number, timing, or position of cells dividing within the mitotic domains.
212 We overexpressed the myristoylated version of Pins instead of using a Pins null mutant because
213 we and others have previously shown that the Pins null mutant causes aberrant asymmetric
214 divisions and our goal was to disrupt Pins polarity while keeping the divisions in-plane (Chanet et
215 al., 2017; Izumi et al., 2004). We have previously shown myristoylated Pins is functional and able
216 to rescue off-axis divisions that occur after Dlg-RNAi (Chanet et al., 2017). Despite occurring in-
217 plane, spindles in embryos expressing myristoylated Pins fail to orient along the AP axis. Instead,
218 division angles are evenly distributed, occurring with seemingly no preference between the DV

219 and AP axes for cells within MD1 (Figure 3I-J, Figure 3- video 2). In comparison, spindles in
220 embryos expressing control Pins orient along the AP axis, with most divisions occurring within
221 30° of the AP axis (Figure 3G-H). Myr-Pins expressing embryos had an average division angle
222 within MD1 that was significantly different from controls (42.7 and 20.1, respectively,
223 p=0.000103). Results for MDs 3 and 5 are consistent with MD1 (Figure 3- figure supplement 3).
224 Myristoylated Pins expression also disrupted division orientation in MD14. Myr-Pins expressing
225 embryos had an average division angle within MD14 that was significantly different from controls
226 (41.2 and 18.1, respectively, p=0.0079) (Figure 3K-N). These data suggest that Pins polarity is
227 necessary for mitotic spindle orientation and planar polarity of divisions within MDs 1, 3, 5, and
228 14. Next we investigated what mechanisms establish Pins planar polarity.
229
230 *Adherens junctions, but not Toll-like receptors or other PCP pathways, are required for division*
231 *orientation.*
232 We hypothesized that Pins polarity could require an upstream planar cell polarity pathway
233 and/or a mechanical cue. We first tested the requirement of planar cell polarity pathways. Some
234 well-known planar polarity pathways include the Fat-Dachsous, the core PCP, and the PAR
235 pathways (Hale and Strutt, 2015; Strutt and Strutt, 2009). The Fat-Dachsous and core PCP
236 pathways were not good candidates for orienting divisions within MDs 1, 3, and, 5 because
237 previous work has shown the components of these pathways are not expressed early enough
238 and/or in the MDs to be involved (Clark et al., 1995; Tomancak et al., 2002; Tomancak et al.,
239 2007). The PAR pathway was also not a good candidate because the *Drosophila* homologue of
240 Par 3, Bazooka (Baz), did not exhibit planar cell polarity in the MDs, despite retaining apical
241 localization during mitosis (Ko et al., 2020). Therefore, we explored the possible involvement of
242 Toll-like receptors (TLRs), which act downstream of even-skipped (Eve) and have been shown to
243 be necessary for the planar polarity of non-muscle myosin II (Myo II) and Baz in the *Drosophila*
244 trunk (Lavalou et al., 2021; Pare et al., 2014). We investigated whether TLRs were involved in

245 division orientation by injecting live embryos with dsRNA of TLRs 2, 6, and 8 and control 0.1x TE
246 buffer. Furthermore, we analyzed fixed embryos that were triple mutants for these TLRs. Injection
247 of dsRNA of TLRs 2, 6, and 8 did not have a significant impact on division orientation (Figure 4 -
248 figure supplement 1 A-D). The triple TLR mutant perturbation was significantly different from
249 controls but, did not randomize division orientation to the extent of expressing Myr-Pins (Figure
250 4- figure supplement 1 E-F). Finally, Myo II and Baz were not planar polarized in the *Drosophila*
251 head (Chanet et al., 2017; Ko et al., 2020), leading us to conclude that TLRs are not solely
252 responsible for division orientation in MDs 1, 3, 5.

253 We next tested the function of AJs. AJs mechanically couple epithelial cells, serve as
254 platforms for protein assembly, and are composed of cadherin-catenin complexes (Hinck et al.,
255 1994; Kovacs and Yap, 2008; Leckband and Prakasam, 2006; Oda et al., 1994; Rimm et al.,
256 1995a; Takeichi, 1991; Yap et al., 1997). AJs are connected to F-actin, which is required for force
257 transmission (Desai et al., 2013; Rimm et al., 1995b; Yonemura et al., 2010). Junctional proteins,
258 such as Canoe/Afadin (cno), have been implicated in spindle positioning (Carminati et al., 2016;
259 Speicher et al., 2008; Wee et al., 2011). Previous work has shown that E-Cadherin is able to
260 recruit Pins in a tension dependent manner (Hart et al., 2017). While AJs are not required for in-
261 plane divisions in certain tissues (Bergstralh et al., 2013), they could serve as platforms for Pins
262 to cue division orientation. To perturb AJs, we maternally depleted α-catenin (αcat) using RNAi.
263 We have shown that αcat depletion is the most severe way to disrupt adherens junctions, totally
264 uncoupling mesoderm cell actomyosin from the junctions, preventing their apical constriction, and
265 lowering adherens junction levels throughout the entire embryo (Denk-Lobnig et al., 2021; Yevick
266 et al., 2019). We crossed the RNAi (hairpin) stock to flies expressing a maternal GAL4 and
267 fluorescently labelled tubulin to visualize spindles. When compared to a control RNAi (Rh3),
268 embryos expressing the αcat RNAi had an even distribution of division angles in MD1, occurring
269 with seemingly no preference between the DV and AP axes. αcat-depleted embryos exhibited an

270 average division angle that was significantly different from controls (36.7 and 26.4, respectively;
271 p=0.000583) (Figure 4A-D, Figure 3- video 2). αcat RNAi also disrupted spindle orientations in
272 MD3 and MD5 (Figure 4- figure supplement 2). Perturbation using αcat RNAi does not
273 recapitulate the complete disruption of division orientation seen in embryos expressing myr-Pins.
274 This is likely due to the inherent variability in the RNAi knockdown. We observed embryos that
275 had severe disruption of division orientation (Figure 4E) and embryos that had minor disruption
276 and appeared more similar to controls (Figure 4F). We found that embryos with greater reductions
277 in adhesion (i.e. more rounded cell morphology) exhibited more severe disruption of division
278 orientation (Figure 4E), consistent with AJs and possibly force transmission being required for
279 spindle orientation.

280 Because Cno has been shown to interact with Pins (Speicher et al., 2008; Wee et al., 2011),
281 we tested Cno function in MDs 1, 3, and 5. To avoid the more catastrophic defects of a *cno* null
282 mutant (Sawyer et al., 2009), we used two RNAi lines to maternally deplete Cno and crossed
283 each to flies expressing fluorescently labelled tubulin. Measuring division angles, as previously
284 described, we found that Cno depletion does not significantly disrupt division orientation within
285 MDs 1, 3, and 5 compared to controls, Cno-depleted embryos exhibited an average division angle
286 that was not significantly different from controls (27.9 and 26.4, respectively; p=0.2698) (Figure
287 4G-H). Note that Cno-RNAi with these lines disrupted myosin localization, similarly to genetic
288 mutants (Sawyer et al., 2011; Sawyer et al., 2009), but did not fully abrogate midline convergence
289 during ventral furrow formation (Jodoin et al., 2015), unlike αcat RNAi (Denk-Lobnig et al., 2021).
290 Together these data suggest a role for AJs and possibly force transmission in spindle orientation.
291 Given our results, we next tested whether AJs were required for polarization of Pins within MDs
292 1, 3, and 5.

293

294 *Disruption of adherens junctions disrupts Pins polarization*

295 To determine whether AJs are involved in Pins planar polarized localization, we examined
296 fluorescently labelled Pins in α-catenin-depleted embryos. In contrast to control embryos, we
297 found that Pins planar polarity is abolished when α-cat was depleted (Figure 5A-D, Figure 5- video
298 1). Pins appeared to have no preferential localization, though given that cells divide in the
299 epithelial plane, a process that depends on Pins, Pins must still localize laterally. Pins peak to
300 trough ratio at the posterior was different in controls compared to α-catenin-depleted embryos
301 (1.33±0.0751 and 1.06±0.0173, respectively, mean and S.D., p=1.1887e-08). These data
302 demonstrate a role for AJs in Pins planar polarization in MD 1.
303
304 *Mechanical cues affect Pins polarization and division orientation*
305 Given our results that AJs are involved in division orientation and Pins polarity and our finding
306 that Pins is planar polarized within the force-dependent oriented divisions of MD14, we
307 hypothesized that force transduction through AJs contributed to Pins polarization and division
308 orientation in MDs 1, 3, and 5. To further test the role of force, we injected embryos expressing
309 fluorescently labelled Pins and tubulin with a low dose of cytochalasin D (CytoD) that we have
310 shown to inhibit force transmission without globally depolymerizing F-actin (Jodoin et al., 2015;
311 Mason et al., 2013). Actomyosin is also necessary for cell rounding, which is necessary for planar
312 divisions for MD cells (Chanet et al., 2017). As we were interested in the orientation of planar
313 divisions, we focused our analysis on divisions that occurred within the plane of the epithelium.
314 We found that injections of CytoD disrupted planar polarized division orientation, CytoD injected
315 embryos exhibited an average division angle that was significantly different from controls (53.7
316 and 21.9, respectively; p=0.0043) (Figure 6B, D, F, H). CytoD injection also disrupted spindle
317 orientations in MD3 and MD5 (Figure 6- figure supplement 1). In addition, Pins localization was
318 disrupted in embryos injected with CytoD whereas Pins exhibited normal polarity in DMSO
319 injected controls (Figure 6A, C, E, G, Figure 5- video 1). The posterior Pins peak to trough ratio

320 was different for DMSO injected controls and CytoD injected embryos (1.17±0.0685 and
321 1.08±0.0609, respectively, mean and S.D., p=6.5007e-11). Interestingly, DMSO injection seemed
322 to perturb the synchrony of divisions. In non-injected embryos, cells within the domain divide in a
323 wave-like pattern, starting in the middle of the domain and propagating to the domain boundary
324 (Di Talia and Wieschaus, 2012). In DMSO injected embryos, nearly all cells round and divide
325 simultaneously. This division timing disruption did not disrupt division orientation or Pins
326 polarization. As CytoD and αcat RNAi have many effects beyond disrupting forces, we next
327 sought to test the role of tissue mechanics without chemical or genetic perturbation.

328 To that end, we performed laser ablation experiments to mechanically isolate MDs from the
329 rest of the tissue. We focused on MD1 and performed a series of four cuts to isolate the domain
330 (Figure 6I). We were unable to look at the effect on Pins polarization because the ablation
331 bleached the Pins::YFP signal. Using embryos that expressed fluorescently labelled tubulin, we
332 analyzed the effect of mechanical isolation on spindle orientation. Cells that divide within the
333 mechanically isolated region fail to orient along the AP axis (Figure 6K, N). As an internal control,
334 we utilized the mirrored spatial pattern of MD1 and cut one side of the domain and left the other
335 side uncut (Figure 6I). In the same embryo, we were able to observe spindles within the cut region
336 fail to orient and neighboring cells outside the cut region orient correctly (Figure 6J, M, Figure 6-
337 video 1). As a further control, and to compensate for the difficulty in acquiring images that
338 permitted visualization of both sides of the domain, we performed sham ablations, where we
339 irradiated the region with a level of light below the cutting threshold. In sham ablated control
340 embryos, spindles oriented with preference towards the AP axis and had an average division
341 angle that was significantly different from cells within the cut region (20.0 and 58.0, respectively;
342 p=0.0286) (Figure 6J - M, Figure 6-figure supplement 2E).

343 To test whether forces transmitted from either cephalic furrow invagination (posterior to MDs)
344 or ventral furrow (ventral to MDs) - mesoderm invagination - are required for oriented divisions,
345 we made directional incisions to separate MD1 from these morphogenetic movements. The

346 cephalic furrow is closest to MDs 1, 3, and 5 and could be expected to pull the MD cells along the
347 AP axis. We made DV oriented (horizontal) laser ablations in the posterior part of MD5 to
348 separate the dorsal head from the cephalic furrow and found that cells exhibited oriented
349 divisions, occurring with an average division angle similar to control sham ablations (18.3 and
350 20.0, respectively; p=1) (Figure 6O, Figure 6-figure supplement 2B, D, E, Figure 6- video 2). In
351 contrast, we found that AP oriented line ablations ventral to the head MDs, which separated them
352 from putative pulling forces from the mesoderm, resulted in a random distribution of division
353 angles, similar to complete isolation of the MD (40.0 and 20.0, respectively; p=0.0286) (Figure
354 6P, Figure 6-figure supplement 2A, C, E, Figure 6- video 2).
355
356 *Mesoderm invagination polarizes Pins and division orientation in the embryonic head*
357 The divisions in MDs 1, 3, and 5 occur during gastrulation, ventral furrow formation pulls
358 ectoderm cells around circumference of the embryo (Lye et al., 2015; Rauzi et al., 2015), and
359 separation of the MDs from the ventral region disrupts division orientation. Therefore, we
360 hypothesized that forces from mesoderm invagination, which occurs ~ 10 minutes before division,
361 could cue Pins polarization and division orientation. To perturb mesoderm invagination, we
362 disrupted the transcription factor Snail because Snail-depletion most severely depletes apical
363 actomyosin activity, and thus pulling force, in the ventral furrow (Martin et al., 2009; Mason et al.,
364 2013). We injected Snail dsRNA into embryos expressing fluorescently labelled tubulin and Pins.
365 We found that Snail depletion disrupted division orientation (Figure 7B, D, F, H, Figure 7- video
366 1). Embryos injected with Snail dsRNA had a random distribution of division angles, occurring
367 with an average division angle significantly different from controls (40.0 and 22.6, respectively;
368 p=0.0121). In addition, Pins polarity was clearly disrupted in embryos injected with Snail dsRNA.
369 For 0.1x TE buffer injected controls, the posterior Pins peak to trough ratio was different from
370 Snail dsRNA injected embryos (1.27±0.08401 and to 1.10±0.10545, respectively, mean and S.D.,
371 p=6.7956e-08) (Figure 7A, C, E, G). Beyond division orientation and Pins polarity, injections of

372 Snail dsRNA disrupted the patterning of MDs 1, 3, and 5. Instead of three distinct domains, a
373 single group of anterior cells divide. Taken together, these data indicate morphogenetic forces
374 play a role in Pins polarity and division orientation within MDs 1, 3, and 5. A role for morphogenetic
375 forces is consistent with our observation that disruption of αcat, actomyosin (with CytoD) or laser
376 ablation disrupt division orientation.
377
378 **Discussion:**
379 Here, we discovered that Pins exhibits planar cell polarity in mitotic domains of the dorsal
380 head (MDs 1, 3, and 5) and along the ventral midline (MD14). We demonstrated that Pins polarity
381 is required for spindle orientation by overexpressing a myristoylated version of Pins that exhibits
382 unregulated cortical localization and disrupts spindle orientation. We found that Pins planar cell
383 polarity and AP spindle orientation depend on adherens junctions. This and our finding that
384 actomyosin disruption also prevents Pins planar cell polarity led us to hypothesize that force
385 transmission through the tissue orients Pins and cell divisions. We showed that forces from ventral
386 furrow formation were critical for spindle orientation, by 1) mechanically isolating MD1 cells from
387 all surrounding tissue (Figure 7I, purple lines), 2) mechanically isolating MD1 cells specifically
388 from the ventral furrow via directional laser ablations (Figure 7I, red lines), and 3) showing that
389 disrupting ventral furrow formation via Snail depletion abrogates proper spindle orientation and
390 Pins localization.
391
392 *Other mechanisms of division orientation*
393 Several other mechanisms of planar polarized division orientation have been identified.
394 Previous works have shown that planar cell polarity pathways, namely the Fat/Dachsous, the core
395 PCP and the PAR pathways, coordinate divisions of the fly wing disc, during Zebrafish
396 gastrulation, and in *Drosophila* sensory organ precursor (SOP) cells, amongst other contexts
397 (Baena-Lopez et al., 2005; Besson et al., 2015; Concha and Adams, 1998; Gho and Schweisguth,

398 1998; Gong et al., 2004; Mao et al., 2006). We ruled out the Fat/Dachsous and core PCP
399 pathways because previous studies indicated the components of these pathways are not
400 expressed early enough in development to play a role in orienting the divisions of the dorsal head
401 or ventral midline (Clark et al., 1995; Tomancak et al., 2002; Tomancak et al., 2007). We further
402 confirmed this by examining fluorescently tagged versions of proteins within these pathways. As
403 was reported, we found no evidence of appreciable expression of these proteins (data not shown).
404 Further, we ruled out the PAR pathway because we saw no evidence of planar polarity in
405 Bazooka/Par 3 (Ko et al., 2020). The Toll-like receptor planar polarity pathway that polarizes
406 myosin in the *Drosophila* trunk was a candidate for involvement in the mitotic domains (Pare et
407 al., 2014). We ruled out this pathway for two reasons, first the TLR pathway in the *Drosophila*
408 trunk results in polarized Myosin and Bazooka/Par3. Observation of these proteins in the dorsal
409 head showed no strong polarization of either protein (Chanet et al., 2017; Ko et al., 2020). Second,
410 we generated a triple mutant of the TLRs identified and performed injections of dsRNA of these
411 TLRs. In each case, spindle orientation was not affected to the extent of the myristoylated Pins
412 perturbation, indicating TLRs cannot be solely responsible for spindle orientation in MDs 1, 3, and
413 5.

414 Hertwig's rule or the long axis rule is perhaps one of the most established mechanisms of
415 division orientation. More recent studies have shown that tricellular junctions are a predictors of
416 division orientation. Mud localizes to tricellular junctions which cues spindle orientation (Bosveld
417 et al., 2016). We did not observe Mud localization to tricellular junctions within the dorsal head
418 mitotic domains and along the ventral midline. Furthermore, we find no correlation between cell
419 long axis and division orientation within these domains, while we find a strong correlation between
420 Pins polarity and cell division angle.

421

422 *Myosin-dependent tension and division orientation*

423 Myosin-dependent tension has been shown to cue the orientation of the mitotic spindle. A
424 growing body of work suggests a role for tension in division orientation, with notable examples in
425 fly development. In the fly notum, it was shown that cells rely on isotropic myosin-dependent
426 tension to sense cell shape and divide along the cell long axis (Lam et al., 2020). Unlike the cells
427 of the fly notum, cells within MDs 1, 3, 5, and 14 do not follow the long axis rule. However, isotropic
428 myosin-dependent tension is required for cell rounding and for symmetric cell divisions in MD
429 cells (Chanet et al., 2017).

430 Tension has also been shown to overrule the long axis rule and orient divisions with the
431 axis of tension rather than the cell long axis. In the follicular epithelium, cortical tension at the
432 apical surface cues planar divisions in a Canoe-dependent manner (Finegan et al., 2019). In this
433 case, Pins and Mud were not planar polarized but rather localized around the entire cell cortex
434 and did not play a role in the planar divisions within the follicular epithelium. Similarly, in
435 parasegmental boundaries, local anisotropy in myosin-dependent tension overrides cell shape.
436 In this context it was shown that tension is both necessary and sufficient to cue division orientation
437 (Scarpa et al., 2018). Pins and Mud were shown to not be involved in division orientation but were
438 necessary for planar divisions. In the head MDs, we did not observe anisotropic myosin-
439 dependent tension. Instead, we observe a uniform distribution of actin and myosin along
440 interfaces of cells. While myosin-dependent tension plays an important role in division orientation
441 in different contexts within fly development, we found no evidence for anisotropic myosin orienting
442 dorsal head divisions.

443

444 *Adherens junctions and division orientation*

445 Prior work suggested that adherens junctions are involved in division orientation. Notably,
446 within *Drosophila* male germline stem cells (Inaba et al., 2010) and sensory organ precursor cells
447 (Le Borgne et al., 2002). The adherens junction component, E-cadherin is localized
448 asymmetrically and coordinates the asymmetric divisions within these cells and perturbation of E-

449 cadherin results in misorientation of the mitotic spindle. Interestingly, in sensory organ precursor
450 cells it was also shown that perturbation of E-cadherin disrupted the Pins localization, although
451 Pins still appears as a crescent (Le Borgne et al., 2002).

452 E-cadherin also has a demonstrated role in symmetric divisions. In MDCK cells E-cadherin
453 recruits Pins in a tension-dependent manner (Hart et al., 2017). It was previously known that
454 Pins/LGN localizes to junctions, but this study first showed a role for force in Pins' junctional
455 localization (Hart et al., 2017). Our findings are consistent with these results. While we did not
456 find a role for Cno in oriented cell division, we were unable to analyze division orientation in a *cno*
457 null mutant, because these mutants also disrupt mesoderm invagination (Sawyer et al., 2009). As
458 seen in the MDCK cells, in cells within the dorsal head mitotic domains and ventral midline
459 adherens junctions may sense anisotropic force or shear forces within the tissue and recruit
460 spindle rotation machinery in a polarized fashion to cue division orientation. Mechanical tension
461 and tissue flow has has been shown to orient other planar cell polarity proteins (Aigouy et al.,
462 2010; Aw et al., 2016). To our knowledge, this is the first *in vivo* example where mechanical force
463 has been shown to polarize Pins to mediate division orientation.

464

465 *Role of divisions in morphogenesis*

466 Whole-embryo light-sheet imaging has revealed a connection between mesoderm
467 invagination and posterior, mediolateral flows in the head (Stern et al., 2022). These flows could
468 explain how large-scale tissue movements on the ventral side of the embryo are connected to
469 oriented division in the dorsal head. An important question that remains is the function of the
470 oriented divisions of the dorsal head during morphogenesis. The oriented divisions of the ventral
471 midline (MD14) have been shown to alleviate tissue strain and promote tissue elongation by
472 promoting an increase in surface area of the mesectoderm (Wang et al., 2017). This agrees with
473 other studies which suggest that oriented division facilitate tissue elongation during development
474 (Aigouy et al., 2010; Baena–Lopez et al., 2005; Gong et al., 2004; Mao et al., 2011). Perturbation

475 using myr-Pins did not affect the number of dividing cells within the domains or the timing of onset
476 of divisions but could possibly affect the elongation of the head epithelium. A recent study followed
477 all the cell intercalations, movements, and divisions during gastrulation, showing cell divisions
478 compensate for the cell loss due to various invaginations (Stern et al., 2022). Indeed, past work
479 has shown that cell division can lead to oriented pushing forces that could contribute to
480 morphogenesis (Gupta et al., 2021). In the embryo, apical relaxation that results from mitotic entry
481 and the following oriented division has been shown to give rise to ectopic tissue folds (Ko et al.,
482 2020). Therefore, we speculate that the oriented division of the dorsal head facilitate tissue
483 elongation and compensate for cell loss from mesoderm and endoderm invagination.
484
485 *Study limitations and future directions*
486 While the evidence in this study supports the hypothesis that morphogenic forces polarize
487 Pins which is required for division orientation, the interpretation of this evidence is limited by
488 certain aspects of the study. First, in describing Pins crescents in mitotic cells, we argue that Pins
489 is on the posterior side for MDs 1 and 3 and anterior side for MD5 (Figure 2A, C, Figure 2- figure
490 supplement 1). This result is based on observation of cells on the boundary of mitotic domains
491 that are not surrounded by other mitotic cells. We do not have the resolution to determine whether
492 Pins is on one or both sides of cells within the domains. One question that arises from this
493 observation is: how does a junction that is under tension recruit Pins to just one side? It will be of
494 future interest to understand the sidedness of Pins in the mitotic domains and what causes this
495 sidedness.
496 A broader question is how Pins is specifically recruited along the AP axis. While we show
497 that mesoderm invagination is necessary for division orientation, what provides the directionality
498 of the divisions remains unknown. Previous work has shown tissue flows that correspond to the
499 division orientations we observe (Streichan et al., 2018). More work is needed to determine the
500 nature of the forces generated at the ventral midline orient divisions in the dorsal head.

Finally, we can only speculate on the significance of these oriented divisions during morphogenesis. Planar, oriented division have been shown to be involved in tissue elongation and folding (Baena–Lopez et al., 2005; Kulukian and Fuchs, 2013; Lancaster and Knoblich, 2012; Morin and Bellaiche, 2011). Given that the divisions of MDs 1, 3, 5, and 14 take place during gastrulation, we hypothesize that the divisions may aid in morphogenic movements such as germ-band extension and cephalic furrow invagination, but we have not directly seen this. These questions will form the basis for future work on the relationship between mechanical and molecular cues in division orientation and the contribution of division orientation during development.

527 **References**

528 Aigouy, B., R. Farhadifar, D.B. Staple, A. Sagner, J.C. Roper, F. Julicher, and S. Eaton. 2010. Cell
529 flow reorients the axis of planar polarity in the wing epithelium of Drosophila. *Cell*.
530 142:773-786.
531 Aw, W.Y., B.W. Heck, B. Joyce, and D. Devenport. 2016. Transient Tissue-Scale Deformation
532 Coordinates Alignment of Planar Cell Polarity Junctions in the Mammalian Skin. *Curr*
533 *Biol*. 26:2090-2100.
534 Baena-Lopez, L.A., A. Baonza, and A. Garcia-Bellido. 2005. The orientation of cell divisions
535 determines the shape of Drosophila organs. *Curr Biol*. 15:1640-1644.
536 Bell, G.P., G.C. Fletcher, R. Brain, and B.J. Thompson. 2015. Aurora kinases phosphorylate Lgl to
537 induce mitotic spindle orientation in Drosophila epithelia. *Curr Biol*. 25:61-68.
538 Bellaïche, Y., A. Radovic, D.F. Woods, C.D. Hough, M.L. Parmentier, C.J. O'Kane, P.J. Bryant, and
539 F. Schweisguth. 2001. The Partner of Inscuteable/Discs-large complex is required to
540 establish planar polarity during asymmetric cell division in Drosophila. *Cell*. 106:355-366.
541 Bergstralh, D.T., H.E. Lovegrove, and D. St Johnston. 2013. Discs large links spindle orientation
542 to apical-basal polarity in Drosophila epithelia. *Curr Biol*. 23:1707-1712.
543 Besson, C., F. Bernard, F. Corson, H. Rouault, E. Reynaud, A. Keder, K. Mazouni, and F.
544 Schweisguth. 2015. Planar Cell Polarity Breaks the Symmetry of PAR Protein Distribution
545 prior to Mitosis in Drosophila Sensory Organ Precursor Cells. *Curr Biol*. 25:1104-1110.
546 Bosveld, F., O. Markova, B. Guirao, C. Martin, Z. Wang, A. Pierre, M. Balakireva, I. Gaugue, A.
547 Ainslie, N. Christophorou, D.K. Lubensky, N. Minc, and Y. Bellaiche. 2016. Epithelial
548 tricellular junctions act as interphase cell shape sensors to orient mitosis. *Nature*.
549 530:495-498.
550 Busson, S., D. Dujardin, A. Moreau, J. Dompierre, and J.R. De Mey. 1998. Dynein and dynactin
551 are localized to astral microtubules and at cortical sites in mitotic epithelial cells. *Curr*
552 *Biol*. 8:541-544.
553 Cabernard, C., and C.Q. Doe. 2009. Apical/basal spindle orientation is required for neuroblast
554 homeostasis and neuronal differentiation in Drosophila. *Dev Cell*. 17:134-141.
555 Campinho, P., M. Behrndt, J. Ranft, T. Risler, N. Minc, and C.P. Heisenberg. 2013. Tension-
556 oriented cell divisions limit anisotropic tissue tension in epithelial spreading during
557 zebrafish epiboly. *Nat Cell Biol*. 15:1405-1414.
558 Carminati, M., S. Gallini, L. Pirovano, A. Alfieri, S. Bisi, and M. Mapelli. 2016. Concomitant
559 binding of Afadin to LGN and F-actin directs planar spindle orientation. *Nat Struct Mol*
560 *Biol*. 23:155-163.
561 Carvalho, C.A., S. Moreira, G. Ventura, C.E. Sunkel, and E. Morais-de-Sá. 2015. Aurora A triggers
562 Lgl cortical release during symmetric division to control planar spindle orientation. *Curr*
563 *Biol*. 25:53-60.
564 Chanet, S., R. Sharan, Z. Khan, and A.C. Martin. 2017. Myosin 2-Induced Mitotic Rounding
565 Enables Columnar Epithelial Cells to Interpret Cortical Spindle Positioning Cues. *Curr*
566 *Biol*. 27:3350-3358 e3353.
567 Choi, W., N.J. Harris, K.D. Sumigray, and M. Peifer. 2013. Rap1 and Canoe/afadin are essential
568 for establishment of apical-basal polarity in the Drosophila embryo. *Mol Biol Cell*.
569 24:945-963.

570 Clark, H.F., D. Brentrup, K. Schneitz, A. Bieber, C. Goodman, and M. Noll. 1995. Dachsous
571 encodes a member of the cadherin superfamily that controls imaginal disc
572 morphogenesis in Drosophila. *Genes Dev*. 9:1530-1542.
573 Classen, A.K., K.I. Anderson, E. Marois, and S. Eaton. 2005. Hexagonal packing of Drosophila
574 wing epithelial cells by the planar cell polarity pathway. *Dev Cell*. 9:805-817.
575 Concha, M.L., and R.J. Adams. 1998. Oriented cell divisions and cellular morphogenesis in the
576 zebrafish gastrula and neurula: a time-lapse analysis. *Development*. 125:983-994.
577 Cox, R.T., C. Kirkpatrick, and M. Peifer. 1996. Armadillo is required for adherens junction
578 assembly, cell polarity, and morphogenesis during Drosophila embryogenesis. *Journal of*
579 *Cell Biology*. 134:133-148.
580 da Silva, S.M., and J.P. Vincent. 2007. Oriented cell divisions in the extending germband of
581 Drosophila. *Development*. 134:3049-3054.
582 Denk-Lobnig, M., J.F. Totz, N.C. Heer, J. Dunkel, and A.C. Martin. 2021. Combinatorial patterns
583 of graded RhoA activation and uniform F-actin depletion promote tissue curvature.
584 *Development*. 148.
585 Desai, R., R. Sarpal, N. Ishiyama, M. Pellikka, M. Ikura, and U. Tepass. 2013. Monomeric alpha-
586 catenin links cadherin to the actin cytoskeleton. *Nat Cell Biol*. 15:261-273.
587 Di Talia, S., and E.F. Wieschaus. 2012. Short-term integration of Cdc25 dynamics controls
588 mitotic entry during Drosophila gastrulation. *Dev Cell*. 22:763-774.
589 Edgar, B.A., and P.H. O'Farrell. 1989. Genetic control of cell division patterns in the Drosophila
590 embryo. *Cell*. 57:177-187.
591 Fielmich, L.E., R. Schmidt, D.J. Dickinson, B. Goldstein, A. Akhmanova, and S. van den Heuvel.
592 2018. Optogenetic dissection of mitotic spindle positioning in vivo. *Elife*. 7.
593 Finegan, T.M., D. Na, C. Cammarota, A.V. Skeeters, T.J. Nadasi, N.S. Dawney, A.G. Fletcher, P.W.
594 Oakes, and D.T. Bergstralh. 2019. Tissue tension and not interphase cell shape
595 determines cell division orientation in the Drosophila follicular epithelium. *EMBO J*. 38.
596 Fink, J., N. Carpi, T. Betz, A. Betard, M. Chebah, A. Azioune, M. Bornens, C. Sykes, L. Fetler, D.
597 Cuvelier, and M. Piel. 2011. External forces control mitotic spindle positioning. *Nat Cell*
598 *Biol*. 13:771-778.
599 Foe, V.E. 1989. Mitotic domains reveal early commitment of cells in Drosophila embryos.
600 *Development*. 107:1-22.
601 Gho, M., and F. Schweisguth. 1998. Frizzled signalling controls orientation of asymmetric sense
602 organ precursor cell divisions in Drosophila. *Nature*. 393:178-181.
603 Gibson, W.T., J.H. Veldhuis, B. Rubinstein, H.N. Cartwright, N. Perrimon, G.W. Brodland, R.
604 Nagpal, and M.C. Gibson. 2011. Control of the mitotic cleavage plane by local epithelial
605 topology. *Cell*. 144:427-438.
606 Gloerich, M., J.M. Bianchini, K.A. Siemers, D.J. Cohen, and W.J. Nelson. 2017. Cell division
607 orientation is coupled to cell-cell adhesion by the E-cadherin/LGN complex. *Nat*
608 *Commun*. 8:13996.
609 Godard, B.G., R. Dumollard, E. Munro, J. Chenevert, C. Hebras, A. McDougall, and C.P.
610 Heisenberg. 2020. Apical Relaxation during Mitotic Rounding Promotes Tension-
611 Oriented Cell Division. *Dev Cell*. 55:695-706 e694.
612 Gonczy, P., and L.S. Rose. 2005. Asymmetric cell division and axis formation in the embryo.
613 *WormBook*:1-20.

614 Gong, Y., C. Mo, and S.E. Fraser. 2004. Planar cell polarity signalling controls cell division
615 orientation during zebrafish gastrulation. *Nature*. 430:689-693.
616 Grill, S.W., and A.A. Hyman. 2005. Spindle positioning by cortical pulling forces. *Dev Cell*. 8:461-
617 465.
618 Gumbiner, B.M. 2005. Regulation of cadherin-mediated adhesion in morphogenesis. *Nat Rev*
619 *Mol Cell Biol*. 6:622-634.
620 Gupta, V.K., S. Nam, D. Yim, J. Camuglia, J.L. Martin, E.N. Sanders, L.E. O'Brien, A.C. Martin, T.
621 Kim, and O. Chaudhuri. 2021. The nature of cell division forces in epithelial monolayers.
622 *J Cell Biol*. 220.
623 Hale, R., and D. Strutt. 2015. Conservation of Planar Polarity Pathway Function Across the
624 Animal Kingdom. *Annual Review of Genetics*. 49:529-551.
625 Harris , T.J.C., and M. Peifer 2005. The positioning and segregation of apical cues during
626 epithelial polarity establishment in Drosophila. *Journal of Cell Biology*. 170:813-823.
627 Hart, K.C., J. Tan, K.A. Siemers, J.Y. Sim, B.L. Pruitt, W.J. Nelson, and M. Gloerich. 2017. E-
628 cadherin and LGN align epithelial cell divisions with tissue tension independently of cell
629 shape. *Proc Natl Acad Sci U S A*. 114:E5845-E5853.
630 Hartenstein, V., and J.A. Campos-Ortega. 1985. Fate-mapping in wild-typeDrosophila
631 melanogaster. *Wilhelm Roux's archives of developmental biology*. 194:181-195.
632 Hartenstein, V., E. Rudloff, and J.A. Campos-Ortega. 1987. The pattern of proliferation of the
633 neuroblasts in the wild-type embryo of Drosophila melanogaster. *Rouxs Arch Dev Biol*.
634 196:473-485.
635 Hertwig, O. 1884. Das Problem der Befruchtung und der Isotropie des Eies, eine Theorie der
636 Vererbung, Jena.
637 Hinck, L., I.S. Näthke, J. Papkoff, and W.J. Nelson. 1994. Dynamics of cadherin/catenin complex
638 formation: novel protein interactions and pathways of complex assembly. *J Cell Biol*.
639 125:1327-1340.
640 Inaba, M., H. Yuan, V. Salzmann, M.T. Fuller, and Y.M. Yamashita. 2010. E-cadherin is required
641 for centrosome and spindle orientation in Drosophila male germline stem cells. *PLoS*
642 *One*. 5:e12473.
643 Izumi, Y., N. Ohta, A. Itoh-Furuya, N. Fuse, and F. Matsuzaki. 2004. Differential functions of G
644 protein and Baz-aPKC signaling pathways in Drosophila neuroblast asymmetric division. *J*
645 *Cell Biol*. 164:729-738.
646 Jodoin, J.N., J.S. Coravos, S. Chanet, C.G. Vasquez, M. Tworoger, E.R. Kingston, L.A. Perkins, N.
647 Perrimon, and A.C. Martin. 2015. Stable Force Balance between Epithelial Cells Arises
648 from F-Actin Turnover. *Dev Cell*. 35:685-697.
649 Johnston, C.A., K. Hirono, K.E. Prehoda, and C.Q. Doe. 2009. Identification of an Aurora-
650 A/PinsLINKER/Dlg spindle orientation pathway using induced cell polarity in S2 cells.
651 *Cell*. 138:1150-1163.
652 Ko, C.S., P. Kalakuntla, and A.C. Martin. 2020. Apical Constriction Reversal upon Mitotic Entry
653 Underlies Different Morphogenetic Outcomes of Cell Division. *Mol Biol Cell*. 31:1663-
654 1674.
655 Kovacs, E.M., and A.S. Yap. 2008. Cell-cell contact: cooperating clusters of actin and cadherin.
656 *Curr Biol*. 18:R667-r669.

657 Kulukian, A., and E. Fuchs. 2013. Spindle orientation and epidermal morphogenesis. *Philos*
658 *Trans R Soc Lond B Biol Sci*. 368:20130016.
659 Kunda, P., N.T. Rodrigues, E. Moeendarbary, T. Liu, A. Ivetic, G. Charras, and B. Baum. 2012.
660 PP1-mediated moesin dephosphorylation couples polar relaxation to mitotic exit. *Curr*
661 *Biol*. 22:231-236.
662 Lam, M.S.Y., A. Lisica, N. Ramkumar, G. Hunter, Y. Mao, G. Charras, and B. Baum. 2020.
663 Isotropic myosin-generated tissue tension is required for the dynamic orientation of the
664 mitotic spindle. *Mol Biol Cell*. 31:1370-1379.
665 Lancaster, M.A., and J.A. Knoblich. 2012. Spindle orientation in mammalian cerebral cortical
666 development. *Curr Opin Neurobiol*. 22:737-746.
667 Lavalou, J., Q. Mao, S. Harmansa, S. Kerridge, A.C. Lellouch, J.M. Philippe, S. Audebert, L.
668 Camoin, and T. Lecuit. 2021. Formation of polarized contractile interfaces by self-
669 organized Toll-8/Cirl GPCR asymmetry. *Dev Cell*. 56:1574-1588 e1577.
670 Le Borgne, R., Y. Bellaiche, and F. Schweisguth. 2002. Drosophila E-cadherin regulates the
671 orientation of asymmetric cell division in the sensory organ lineage. *Curr Biol*. 12:95-104.
672 Lechler, T., and E. Fuchs. 2005. Asymmetric cell divisions promote stratification and
673 differentiation of mammalian skin. *Nature*. 437:275-280.
674 Leckband, D., and A. Prakasam. 2006. Mechanism and dynamics of cadherin adhesion. *Annu*
675 *Rev Biomed Eng*. 8:259-287.
676 Legoff, L., H. Rouault, and T. Lecuit. 2013. A global pattern of mechanical stress polarizes cell
677 divisions and cell shape in the growing Drosophila wing disc. *Development*. 140:4051-
678 4059.
679 Lye, C.M., G.B. Blanchard, H.W. Naylor, L. Muresan, J. Huisken, R.J. Adams, and B. Sanson. 2015.
680 Mechanical Coupling between Endoderm Invagination and Axis Extension in Drosophila.
681 *PLoS Biol*. 13:e1002292.
682 Mao, Y., C. Rauskolb, E. Cho, W.L. Hu, H. Hayter, G. Minihan, F.N. Katz, and K.D. Irvine. 2006.
683 Dachs: an unconventional myosin that functions downstream of Fat to regulate growth,
684 affinity and gene expression in Drosophila. *Development*. 133:2539-2551.
685 Mao, Y., A.L. Tournier, P.A. Bates, J.E. Gale, N. Tapon, and B.J. Thompson. 2011. Planar
686 polarization of the atypical myosin Dachs orients cell divisions in Drosophila. *Genes Dev*.
687 25:131-136.
688 Mao, Y., A.L. Tournier, A. Hoppe, L. Kester, B.J. Thompson, and N. Tapon. 2013. Differential
689 proliferation rates generate patterns of mechanical tension that orient tissue growth.
690 *EMBO J*. 32:2790-2803.
691 Martin, A.C., M. Kaschube, and E.F. Wieschaus. 2009. Pulsed contractions of an actin–myosin
692 network drive apical constriction. *Nature*. 457:495-499.
693 Mason, F.M., M. Tworoger, and A.C. Martin. 2013. Apical domain polarization localizes actin-
694 myosin activity to drive ratchet-like apical constriction. *Nat Cell Biol*. 15:926-936.
695 Matsumura, S., T. Kojidani, Y. Kamioka, S. Uchida, T. Haraguchi, A. Kimura, and F. Toyoshima.
696 2016. Interphase adhesion geometry is transmitted to an internal regulator for spindle
697 orientation via caveolin-1. *Nat Commun*. 7:ncomms11858.
698 Minc, N., D. Burgess, and F. Chang. 2011. Influence of cell geometry on division-plane
699 positioning. *Cell*. 144:414-426.

700 Morin, X., and Y. Bellaiche. 2011. Mitotic spindle orientation in asymmetric and symmetric cell
701 divisions during animal development. *Dev Cell*. 21:102-119.
702 Nakajima, Y., E.J. Meyer, A. Kroesen, S.A. McKinney, and M.C. Gibson. 2013. Epithelial junctions
703 maintain tissue architecture by directing planar spindle orientation. *Nature*. 500:359-
704 362.
705 Nestor-Bergmann, A., G.A. Stooke-Vaughan, G.K. Goddard, T. Starborg, O.E. Jensen, and S.
706 Woolner. 2019. Decoupling the Roles of Cell Shape and Mechanical Stress in Orienting
707 and Cueing Epithelial Mitosis. *Cell Rep*. 26:2088-2100 e2084.
708 Nguyen-Ngoc, T., K. Afshar, and P. Gonczy. 2007. Coupling of cortical dynein and G alpha
709 proteins mediates spindle positioning in Caenorhabditis elegans. *Nat Cell Biol*. 9:1294-
710 1302.
711 Oda, H., T. Uemura, Y. Harada, Y. Iwai, and M. Takeichi. 1994. A Drosophila homolog of cadherin
712 associated with armadillo and essential for embryonic cell-cell adhesion. *Dev Biol*.
713 165:716-726.
714 Pare, A.C., A. Vichas, C.T. Fincher, Z. Mirman, D.L. Farrell, A. Mainieri, and J.A. Zallen. 2014. A
715 positional Toll receptor code directs convergent extension in Drosophila. *Nature*.
716 515:523-527.
717 Rauzi, M., U. Krzic, T.E. Saunders, M. Krajnc, P. Ziherl, L. Hufnagel, and M. Leptin. 2015. Embryo-
718 scale tissue mechanics during Drosophila gastrulation movements. *Nature*
719 *Communications*. 6:8677.
720 Rimm, D.L., E.R. Koslov, P. Kebriaei, C.D. Cianci, and J.S. Morrow. 1995a. Alpha 1(E)-catenin is an
721 actin-binding and -bundling protein mediating the attachment of F-actin to the
722 membrane adhesion complex. *Proceedings of the National Academy of Sciences of the*
723 *United States of America*. 92:8813-8817.
724 Rimm, D.L., E.R. Koslov, P. Kebriaei, C.D. Cianci, and J.S. Morrow. 1995b. Alpha 1(E)-catenin is an
725 actin-binding and -bundling protein mediating the attachment of F-actin to the
726 membrane adhesion complex. *Proc Natl Acad Sci U S A*. 92:8813-8817.
727 Sawyer, J.K., W. Choi, K.C. Jung, L. He, N.J. Harris, and M. Peifer. 2011. A contractile actomyosin
728 network linked to adherens junctions by Canoe/afadin helps drive convergent
729 extension. *Mol Biol Cell*. 22:2491-2508.
730 Sawyer, J.K., N.J. Harris, K.C. Slep, U. Gaul, and M. Peifer. 2009. The Drosophila afadin
731 homologue Canoe regulates linkage of the actin cytoskeleton to adherens junctions
732 during apical constriction. *J Cell Biol*. 186:57-73.
733 Scarpa, E., C. Finet, G.B. Blanchard, and B. Sanson. 2018. Actomyosin-Driven Tension at
734 Compartmental Boundaries Orients Cell Division Independently of Cell Geometry In
735 Vivo. *Dev Cell*. 47:727-740 e726.
736 Schaefer, M., A. Shevchenko, A. Shevchenko, and J.A. Knoblich. 2000. A protein complex
737 containing Inscuteable and the Galpha-binding protein Pins orients asymmetric cell
738 divisions in Drosophila. *Curr Biol*. 10:353-362.
739 Siller, K.H., C. Cabernard, and C.Q. Doe. 2006. The NuMA-related Mud protein binds Pins and
740 regulates spindle orientation in Drosophila neuroblasts. *Nat Cell Biol*. 8:594-600.
741 Siller, K.H., and C.Q. Doe. 2008. Lis1/dynactin regulates metaphase spindle orientation in
742 Drosophila neuroblasts. *Dev Biol*. 319:1-9.

743 Speicher, S., A. Fischer, J. Knoblich, and A. Carmena. 2008. The PDZ protein Canoe regulates the
744 asymmetric division of Drosophila neuroblasts and muscle progenitors. *Curr Biol*.
745 18:831-837.
746 Stern, T., S.Y. Shvartsman, and E.F. Wieschaus. 2022. Deconstructing gastrulation at single-cell
747 resolution. *Current Biology*. 32:1861-1868.e1867.
748 Streichan, S.J., M.F. Lefebvre, N. Noll, E.F. Wieschaus, and B.I. Shraiman. 2018. Global
749 morphogenetic flow is accurately predicted by the spatial distribution of myosin motors.
750 *Elife*. 7.
751 Strutt, H., and D. Strutt. 2009. Asymmetric localisation of planar polarity proteins: Mechanisms
752 and consequences. *Semin Cell Dev Biol*. 20:957-963.
753 Takeichi, M. 1991. Cadherin cell adhesion receptors as a morphogenetic regulator. *Science*.
754 251:1451-1455.
755 Tepass, U. 1997. Epithelial differentiation in Drosophila. *Bioessays*. 19:673-682.
756 Thery, M., A. Jimenez-Dalmaroni, V. Racine, M. Bornens, and F. Julicher. 2007. Experimental
757 and theoretical study of mitotic spindle orientation. *Nature*. 447:493-496.
758 Thery, M., V. Racine, A. Pepin, M. Piel, Y. Chen, J.B. Sibarita, and M. Bornens. 2005. The
759 extracellular matrix guides the orientation of the cell division axis. *Nat Cell Biol*. 7:947-
760 953.
761 Tomancak, P., A. Beaton, R. Weiszmann, E. Kwan, S. Shu, S.E. Lewis, S. Richards, M. Ashburner,
762 V. Hartenstein, S.E. Celniker, and G.M. Rubin. 2002. Systematic determination of
763 patterns of gene expression during Drosophila embryogenesis. *Genome Biol*.
764 3:Research0088.
765 Tomancak, P., B.P. Berman, A. Beaton, R. Weiszmann, E. Kwan, V. Hartenstein, S.E. Celniker,
766 and G.M. Rubin. 2007. Global analysis of patterns of gene expression during Drosophila
767 embryogenesis. *Genome Biol*. 8:R145.
768 Tsou, M.F., W. Ku, A. Hayashi, and L.S. Rose. 2003. PAR-dependent and geometry-dependent
769 mechanisms of spindle positioning. *J Cell Biol*. 160:845-855.
770 Wang, M.F., M.V. Hunter, G. Wang, C. McFaul, C.M. Yip, and R. Fernandez-Gonzalez. 2017.
771 Automated cell tracking identifies mechanically oriented cell divisions during Drosophila
772 axis elongation. *Development*. 144:1350-1361.
773 Wang, Q., and B. Margolis. 2007. Apical junctional complexes and cell polarity. *Kidney Int*.
774 72:1448-1458.
775 Wee, B., C.A. Johnston, K.E. Prehoda, and C.Q. Doe. 2011. Canoe binds RanGTP to promote
776 Pins(TPR)/Mud-mediated spindle orientation. *J Cell Biol*. 195:369-376.
777 Wyatt, T.P., A.R. Harris, M. Lam, Q. Cheng, J. Bellis, A. Dimitracopoulos, A.J. Kabla, G.T. Charras,
778 and B. Baum. 2015. Emergence of homeostatic epithelial packing and stress dissipation
779 through divisions oriented along the long cell axis. *Proc Natl Acad Sci U S A*. 112:5726-
780 5731.
781 Yap, A.S., W.M. Brieher, and B.M. Gumbiner. 1997. Molecular and functional analysis of
782 cadherin-based adherens junctions. *Annu Rev Cell Dev Biol*. 13:119-146.
783 Yevick, H.G., P.W. Miller, J. Dunkel, and A.C. Martin. 2019. Structural Redundancy in
784 Supracellular Actomyosin Networks Enables Robust Tissue Folding. *Dev Cell*. 50:586-598
785 e583.

786 Yonemura, S., Y. Wada, T. Watanabe, A. Nagafuchi, and M. Shibata. 2010. alpha-Catenin as a
787 tension transducer that induces adherens junction development. *Nat Cell Biol*. 12:533-
788 542.
789 Yu, F., C.T. Kuo, and Y.N. Jan. 2006. Drosophila neuroblast asymmetric cell division: recent
790 advances and implications for stem cell biology. *Neuron*. 51:13-20.
791
792
793
794
795
796
797
798
799
800
801
802
803
804
805
806
807
808
809
810
811
812
813

Materials and Methods

Fly stocks and genetics

Fly stocks and crosses used in this study are listed in Supplemental Table S1. Crosses were maintained at 25°C. In the F1 generation, non-balancer females and males were used to set up cages that were incubated at 25°C. The F2 generation was used for imaging.

Live and fixed imaging

For live imaging, embryos were dechorionated in 50% bleach for 2 minutes, washed in water, and mounted onto a glass slide coated with embryo glue (double-sided tape dissolved in heptane). No. 1.5 coverslips coated in glue were attached to the slide to use as spacers and a No. 1 coverslip was attached on top to create a chamber. Halocarbon 27 oil was used to fill the chamber. All imaging took place at 23-25°C.

For imaging fixed embryos, embryos were dechorionated in 50 % bleach (Chlorox) for 2 minutes, washed in water, and then fixed in 4% paraformaldehyde (Electron Microscopy Sciences) in 0.1 M phosphate buffer at pH 7.4 with 50% heptane (Alfa Aesar) for 30 min and manually devitellinized (TLR stains) or devitellinized by removing fixative, adding 50% methanol (Sigma Aldrich), and vortexing (Pins and Mud). Manually devitellinized embryos were stored in 0.01% Tween 20 in PBS (PBS-T and embryos devitellinized with 50% methanol were stored in 100% methanol at −4°C and rehydrated in PBS-T.

Embryos were washed in PBS-T, blocked with 10% BSA in PBS-T, and incubated with antibodies diluted in PBS-T. Embryos were incubated with primary antibodies at room temperature for 2 h. Antibodies used in this study are listed in Supplemental Table S1. Secondary antibodies used were conjugated with Alexa Fluor 488, 568, or 647 (Invitrogen) diluted at 1:500 in 5% BSA in PBS-T incubated overnight at 4°C. After antibody incubation, embryos were mounted onto glass slides using AquaPolymount (Polysciences).

All images were taken on a Zeiss LSM 710 confocal microscope with a 40×/1.2 Apochromat water objective lens, an argon-ion, 561-nm diode, 594-nm HeNe, 633 HeNe laser, and Zen software. The pinhole was set to 1 airy unit (au) for fixed imaging and 2.5 au for live imaging. For two-color live imaging, band-pass filters were set at ~490–565 nm for GFP and ~590–690 nm for mCherry (mCh). For three-color imaging, band-pass filters were set at ~480–560 nm for Alexa Fluor 488, ~580–635 nm for Alexa Fluor 568, and ~660–750 nm for Alexa Fluor 647.

dsRNA injections

Primers included the sequence of the T7 promoter (TAATACGACTCACTATAGGGAGACCAC) followed by the following recognition sequences:
Toll 2 F: AGTTTGAATCGAAACGCGAG
Toll 2 R: GGACACTGCACCGGATGT
Toll 6 F: ATCGGCCAAAAAGAGCAGTA
Toll 6 R: AGCAGCGTGTGCAGATTATT
Toll 8 F: ATGCGTACCATTTTCCTACCA
Toll 8 R: TTTTTACTCTTCGCTTTTTCGC
Snα–F: CGGAACCGAAACGTGACTAT
Snα–R: GCGGTAGTTTTTGGCATGAT

Primer pairs were used to amplify a PCR product from genomic DNA. PCR products were directly used in a transcription reaction with T7 polymerase using the MEGAscript transcription kit (Ambion). The reaction was placed in boiling water and allowed to cool to room temperature to

promote annealing. RNA was extracted with phenol:chloroform, washed with ethanol, and resuspended in 0.1M TE buffer.

Stage 2 embryos were dechorionated in 50% bleach for 2 minutes. The embryos were mounted onto glass slides and desiccated for 4 min using Drierite. Embryos were covered with a 3:1 mixture of halocarbon 700/halocarbon 27 oils and then injected laterally. Embryos were imaged 3 hours after injecting.

Drug injections

Embryos were dechorionated in 50% bleach for 2 minutes. The embryos were mounted onto glass slides and desiccated for 4 min using Drierite. Embryos were covered with a 3:1 mixture of halocarbon 700/halocarbon 27 oils and then injected laterally at the beginning of cephalic furrow formation. To disrupt F-actin we resuspended CtyoD (Enzo Life Sciences) at 0.125 mg/ml in DMSO. Embryos were imaged 3-5 minutes after injecting.

Laser ablation

Laser ablations were performed using a 2-photon Mai-Tai laser set to 800 nm on a LSM710 confocal microscope (Zeiss) through a 40x/1.1 objective, using the Zen software (Zeiss) (W. M. Keck Microscopy Facility, Cambridge, MA). For ablations, laser power was set at 20%, with a scan speed of 1.58 ms/px. Ablations were performed with four overlapping linear ROIs around one side of MD1.

Sham ablations were performed with the same setup as the laser ablations except the laser power was set at 10%. This caused the ROIs to become bleached, but not ablated.

Image processing and analysis

All figure images were processed using MATLAB (MathWorks) and FIJI (http://fiji.sc/wiki/index.php/Fiji). A Gaussian smoothing filter (kernel = 0.75 pixel) was applied to all figure images. Brightness and contrast were adjusted to optimally visualize the mitotic spindle or Pins crescents in figure images. Control and experimental images were adjusted the same.

Division angle analysis

Division angle was taken using the angle tool in FIJI and measured as the angle between spindle poles axis and the AP axis in mitotic cells at anaphase or later. The angle values range from 0 degrees, indicating alignment along AP, to 90 degrees, indicating alignment along DV. Unless otherwise stated, 10 embryos and between 100-250 spindles were counted of each genotype. Resulting angles were plotted in rose plots, with percentage of spindles on the r axis and angle on the theta axis.

Intensity profile analysis

Intensity profiles were taken using the segmented line tool in Fiji with a line width of 2 and measured using the Plot Profile feature in Fiji. The perimeter of the cell was outlined starting at the apical most point of mitotic cells in anaphase. The direction of the lines was toward the dorsal midline or ventral midline (clockwise for the left half of the domains and counterclockwise for the right half of the domains). Intensity was normalized to cytoplasmic intensity, which was measured as the mean grey value of a line drawn through the cytoplasm. Unless otherwise stated, 10 cells per embryo and 3 embryos per genotype were analyzed, averaged, and graphed as line plots with normalized intensity on the y axis and distance from start on the x axis.

For statistical analysis, we found the point of maximum Pins intensity and averaged the troughs to either side of this point to get a peak to trough ratio for each cell and then compared this to the ratio achieved by using the corresponding points for Gap43. In experiments with control and

experimental, the peak to trough ratio was found for the control and compared to the ratio achieved by using corresponding points in the experimental condition.

Anisotropy analysis

Aspect ratios of interphase cells were taken using the polygon tool in Fiji and the Fit Ellipse measurement, which gives the major axis length, the minor axis, and the angle of the major axis. Aspect ratio is ratio between the major axis and the minor axis. The average aspect ratio was recorded and the angle of the major axis was compared to the axis of division. Unless otherwise stated, 10 cells per embryo and 3 embryos per genotype were analyzed.

Quantification and statistical analysis

Statistical analyses were performed using the MATLAB statistics toolbox. p values were calculated using a two-sample Mann-Whitney test, the reference sample is the angle distribution in wild-type. Correlation coefficients r are Spearman correlation coefficient. p values are calculated against the null hypothesis r = 0.

Figure Legends

Figure 1. Early mitotic domains in the *Drosophila* head exhibit spindle rotation and oriented division (A) Schematic of the dorsal head of a *Drosophila* embryo with mitotic domain 1 (MD1) in red, mitotic domain 3 (MD3) in blue, and mitotic domain 5 (MD5) in orange. Anterior-posterior (AP) axis is indicated by arrow, the top of images will consistently be anterior, as in the schematic. (B) Image of the dorsal head of a live *Drosophila* embryo expressing CLIP170::GFP to label microtubules/spindle (greyscale). CLIP170::GFP signal is detected in image. MD1 is outlined in red, MD3 in blue, and MD5 in orange, scalebar is 50 µm. (C) MD1 cells exhibit planar polarized cell division. Left, Image of MD1 in live embryo showing labeled myosin (greyscale, Sqh::mCherry), to show cytokinetic rings, and labeled F-actin (green, UtrABD::GFP) to show cell cortex, scalebar is 10 µm. Right, Same image of MD1 annotated with black lines marking the cytokinetic ring of each dividing cell and magenta dashed lines marking division angle. (D) MD1 cells exhibit spindle rotation and alignment. Images are time series of MD1 with CLIP170::GFP marking the mitotic spindle (greyscale), blue lines indicate spindles still rotating and magenta lines represent spindle that have reached their final orientation, scalebar is 10 µm. (E) Schematic of division angle analysis. Division angle is taken with respect to the AP axis such that angle of 0 indicates alignment with the AP axis. Note only spindles during or after anaphase, when division angle is fixed, are measured. (F-H) Rose plots indicating division angles of MD1 (F), MD3 (G), and MD5 (H). Red lines indicate mean division angle. Mean division angle for MD=21.6°, MD3=20.4°, and MD5=19.0°. For MD1, n=10 embryos and 200 spindles, MD3, n=5, embryos and 123 spindles and MD5, n=5 embryos and 140 spindles. (I-J) Rose plots indicating division angles of left (I) or right (J) side of MD1. For left side, n=5 embryos and 100 spindles and right side, n=5 embryos and 103 spindles.

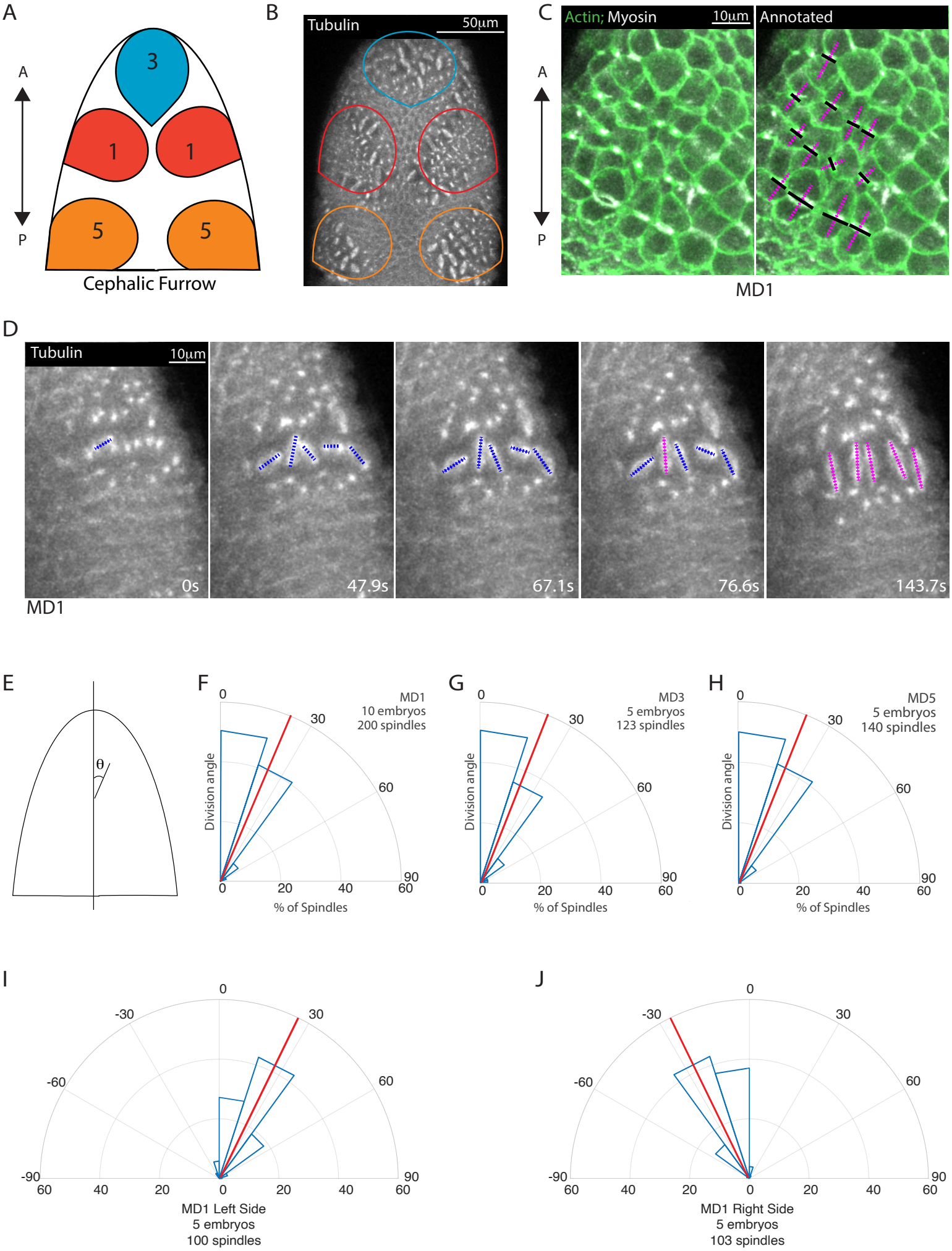
A
A
P
3
1
1
5
5
Cephalic Furrow
B
Tubulin
50µm
C
Actin; Myosin
10µm
Annotated
A
P
MD1
D
Tubulin
10µm
0s
47.9s
67.1s
76.6s
143.7s
MD1
E
θ
F
MD1
10 embryos
200 spindles
Division angle
% of Spindles
G
MD3
5 embryos
123 spindles
Division angle
% of Spindles
H
MD5
5 embryos
140 spindles
Division angle
% of Spindles
I
MD1 Left Side
5 embryos
100 spindles
J
MD1 Right Side
5 embryos
103 spindles

Figure 2. Pins is planar polarized in mitotic domain cells. (A-B) Time series of MD1 of embryo expressing Pins::YFP, to label spindle rotation machinery, and Gap43::mCherry, to mark membranes. scalebar is 10 µm. (C, J) Quantification of average cellular (7-9 cells) Pins::YFP signal intensity around the mitotic cell cortex for 3 separate embryos, lines indicate average of cells in each embryo for MD1 (C) or MD14 (J). Cortical intensity was measured at anaphase, indicated by cell elongation, and normalized to cytoplasmic Pins::YFP signal. (C', J') Average of embryos in C or J. (D, K) Quantification of Gap43::mCherry (membrane marker) intensity for same cells and 3 embryos as in C for MD1 or J for MD14. (D', K') Average of embryos in D, MD1, or K, MD14. Intensity was normalized to cytoplasmic Gap43::mCherry signal. (E) Fixed sample of metaphase cells in MD1 stained for Tubulin (Left), Ecadherin (center), and Pins (Right). (F) Fixed sample of anaphase cells in MD1 stained for Tubulin (Left), Pins (Right). (G) Fixed sample of anaphase cells in MD1 stained for Tubulin (Left) and Mud (Right). (H-I) Time series of MD14 cells expressing Pins::YFP and Gap43::mCherry, similar to A and B. scalebar is 10 µm.

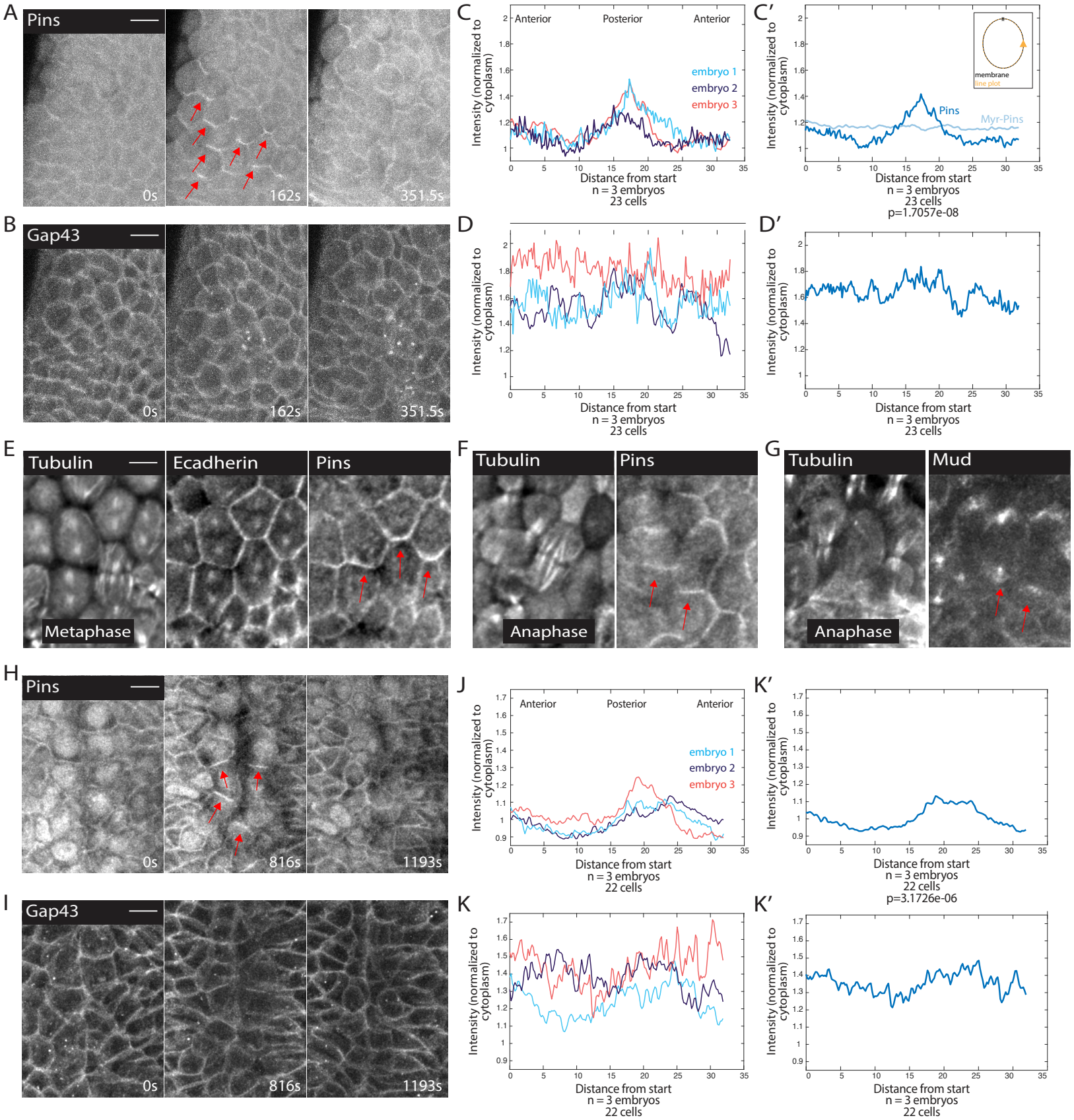
A
Pins
0s
162s
351.5s
B
Gap43
0s
162s
351.5s
C
Anterior
Posterior
Anterior
embryo 1
embryo 2
embryo 3
Intensity (normalized to cytoplasm)
Distance from start
n = 3 embryos
23 cells
C′
membrane
line plot
Pins
Myr-Pins
Intensity (normalized to cytoplasm)
Distance from start
n = 3 embryos
23 cells
p=1.7057e-08
D
Intensity (normalized to cytoplasm)
Distance from start
n = 3 embryos
23 cells
D′
Intensity (normalized to cytoplasm)
Distance from start
n = 3 embryos
23 cells
E
Tubulin
Ecadherin
Pins
Metaphase
F
Tubulin
Pins
Anaphase
G
Tubulin
Mud
Anaphase
H
Pins
0s
816s
1193s
I
Gap43
0s
816s
1193s
J
Anterior
Posterior
Anterior
embryo 1
embryo 2
embryo 3
Intensity (normalized to cytoplasm)
Distance from start
n = 3 embryos
22 cells
K′
Intensity (normalized to cytoplasm)
Distance from start
n = 3 embryos
22 cells
p=3.1726e-06
K
Intensity (normalized to cytoplasm)
Distance from start
n = 3 embryos
22 cells
K′
Intensity (normalized to cytoplasm)
Distance from start
n = 3 embryos
22 cells

Figure 3. Planar polarized divisions depend on asymmetric Pins localization (A-B) Pins localizes in planar polarized crescents immediately prior to spindle orientation. Images are time series of MD1 of embryo with labeled Pins (Pins::YFP) and labeled tubulin (Tubulin::mCherry), to mark mitotic spindles, blue lines indicate spindles that are still rotating, magenta lines indicate spindles that have reached their final orientation. Colored boxes at tips of lines label spindles with the color marking the same spindle at each time point. Scalebar is 10 µm. (C) Spindle orientation is correlated with Pins polarity. Plot of the correlation between the angle of maximum Pins::YFP intensity and division angle., R^2=0.77. (D) Schematic of MD 14, located on either side of the ventral midline (VM). (E-F) Images are a time series of MD14 cells labeled with Pins::YFP and tubulin::mCherry, to mark mitotic spindles. (G, I) Myristoylated Pins disrupts division orientation. Left, image of MD1 of control embryo (G, UAS>PinsGFP) or MD1 of Myristoylated Pins expressing embryo (I, UAS>myr::Pins::GFP). Images show marker (CLIP170::GFP) to mark mitotic spindles (greyscale), scalebar is 10 µm. Right, same image annotated with dashed lines to indicate spindle position. (H, J) Quantification of spindle angles for control embryos (H, UAS>PinsGFP) using rose plots or Myristoylated Pins expressing embryos (J, UAS>myr::Pins::GFP). For control embryos (H, UAS-PinsGFP) MD1, n=7 embryos and 175 spindles. For Myristoylated Pins expressing embryos, n=10 embryos and 284 spindles. Average orientation angles per embryo were statistically different between control and Myristoylated Pins expressing embryos, Mann-Whitney, p=0.000103. (K, M) Pins asymmetry is required for MD14 spindle orientation. Left, image of MD14 of control embryo (G, UAS-PinsGFP) or MD14 of Myristoylated Pins expressing embryo (I, UAS>myr::Pins::GFP). Images show marker (CLIP170::GFP) to mark mitotic spindles (greyscale), scalebar is 10 µm. Right, same image annotated with dashed lines to indicate spindle position. (L, N) Quantification of spindle angles for control embryos (UAS>PinsGFP) or Myristoylated Pins expressing embryos (N, UAS>myr::Pins::GFP) using rose plots. For control embryos (L, UAS>PinsGFP) MD14, n=5 embryos and 97 spindles. For Myristoylated Pins expressing embryos, n=5 embryos and 78 spindles. Average orientation angles per embryo were statistically different between control and Myristoylated Pins expressing embryos, Mann-Whitney, p=0.0079.

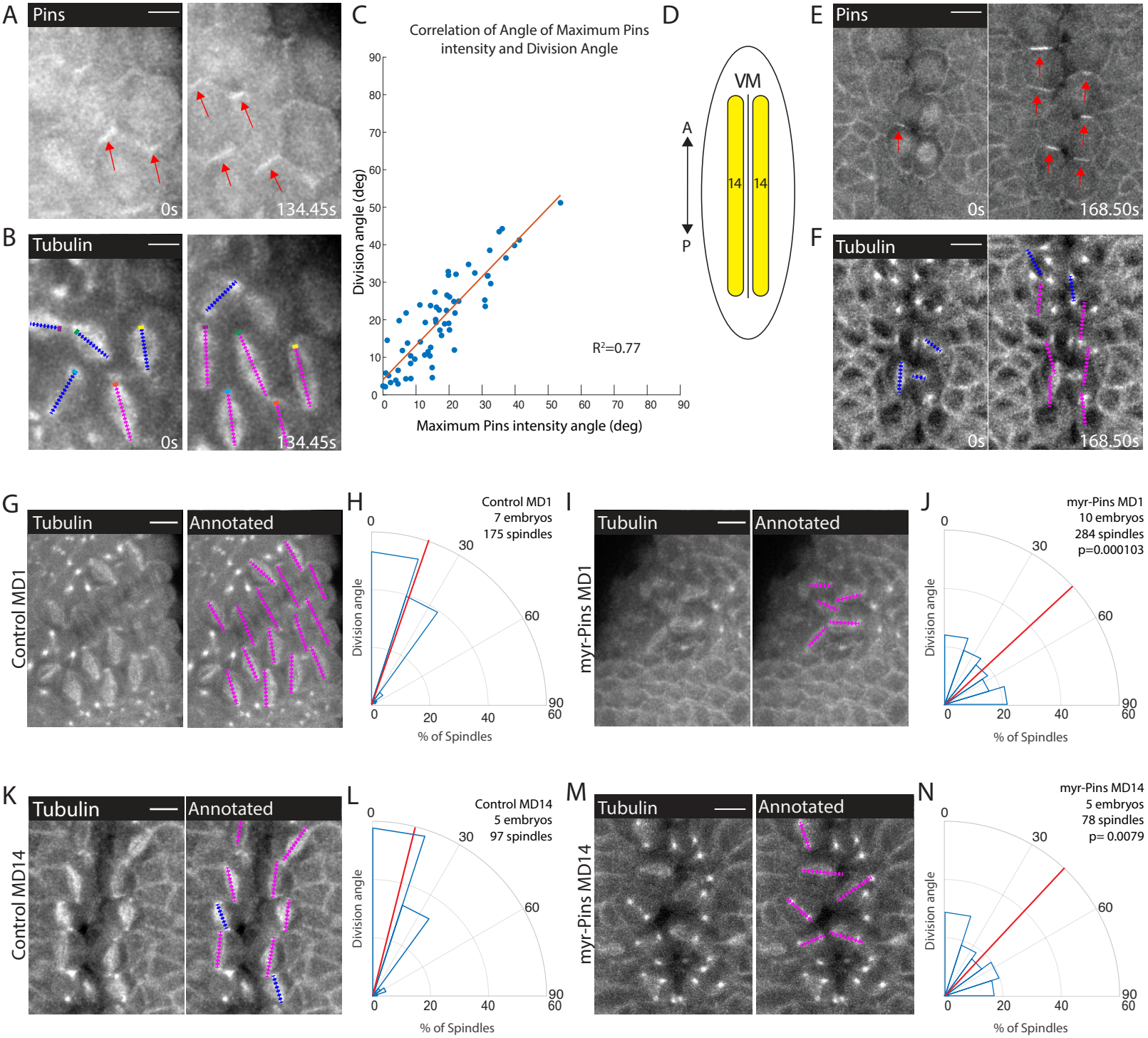
A
Pins
0s
134.45s
B
Tubulin
0s
134.45s
C
Correlation of Angle of Maximum Pins intensity and Division Angle
Division angle (deg)
Maximum Pins intensity angle (deg)
R²=0.77
D
VM
A
P
14
14
E
Pins
0s
168.50s
F
Tubulin
0s
168.50s
G
Tubulin
Annotated
Control MD1
H
Control MD1
7 embryos
175 spindles
Division angle
% of Spindles
I
Tubulin
Annotated
myr-Pins MD1
J
myr-Pins MD1
10 embryos
284 spindles
p=0.000103
Division angle
% of Spindles
K
Tubulin
Annotated
Control MD14
L
Control MD14
5 embryos
97 spindles
Division angle
% of Spindles
M
Tubulin
Annotated
myr-Pins MD14
N
myr-Pins MD14
5 embryos
78 spindles
p= 0.0079
Division angle
% of Spindles

Figure 4. Disruption of adherens junctions, but not Canoe, inhibits planar polarized division orientation (A, C, G) α–catenin depletion disrupts division orientation. Left, image of MD1 of control knock-down (A, Rh3 RNAi), MD1 of α–catenin depleted embryo (C, α–catenin RNAi), or MD1 of Canoe depleted embryo (G, Canoe RNAi). Images show marker (CLIP170::GFP) to mark mitotic spindles (greyscale), scalebar is 10 µm. Right, same image annotated with dashed lines to indicate spindle position. (B, D, H) Quantification of spindle angles for control embryos (B, Rh3 RNAi), α–catenin depleted embryos (D, α–catenin RNAi), or Canoe depleted embryos (H, Canoe RNAi) using rose plots. For control embryos (Rh3 RNAi) MD1, n=10 embryos and 355 spindles. For α–catenin RNAi MD1, n=10 embryos and 248 spindles. For Canoe RNAi MD1, n=7 embryos and 166 spindles. Average orientation angles per embryo were statistically different between control and α–catenin RNAi, Mann-Whitney, p=0.000583, but not for canoe RNAi, Mann-Whitney, p=0.2698. (E-F) Quantification of spindle angles for individual α–catenin depleted embryos using rose plots.

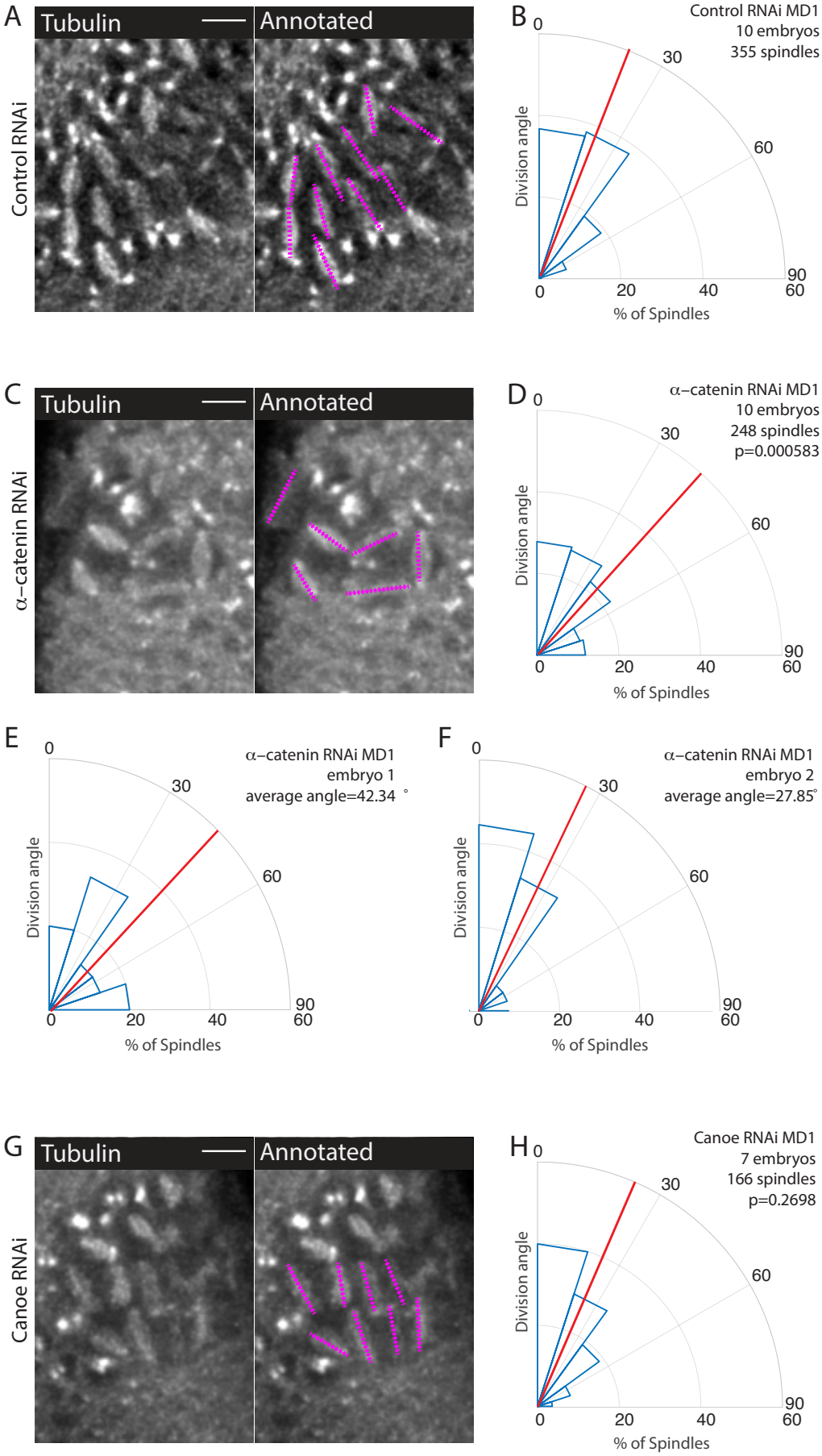
A
Tubulin
Annotated
Control RNAi
B
Control RNAi MD1
10 embryos
355 spindles
Division angle
% of Spindles
C
Tubulin
Annotated
α–catenin RNAi
D
α–catenin RNAi MD1
10 embryos
248 spindles
p=0.000583
Division angle
% of Spindles
E
α–catenin RNAi MD1
embryo 1
average angle=42.34 °
Division angle
% of Spindles
F
α–catenin RNAi MD1
embryo 2
average angle=27.85°
Division angle
% of Spindles
G
Tubulin
Annotated
Canoe RNAi
H
Canoe RNAi MD1
7 embryos
166 spindles
p=0.2698
Division angle
% of Spindles

Figure 5. Adherens junction depletion disrupts Pins planar cell polarity. (A, C) α–catenin depletion disrupts Pins localization. Left, image of a MD1 cell of control embryo (A, Rh3 RNAi) or a MD1 cell of α–catenin depleted embryo (C, α–catenin RNAi). Images show labelled Pins (Pins::YFP), scalebar is 10 μm. Right, same image annotated with dashed line to indicate cell outline used to plot intensity profile, * to indicate start, and arrow to indicate direction of line. (B, D) Quantification of Pins intensity for control embryos (Rh3 RNAi) or α–catenin depleted embryos (D, α–catenin RNAi). Intensity was normalized to cytoplasm. For control (Rh3) MD1, n=3 embryos and 25 cells. For α–catenin RNAi MD1, n=3 and 30 cells.

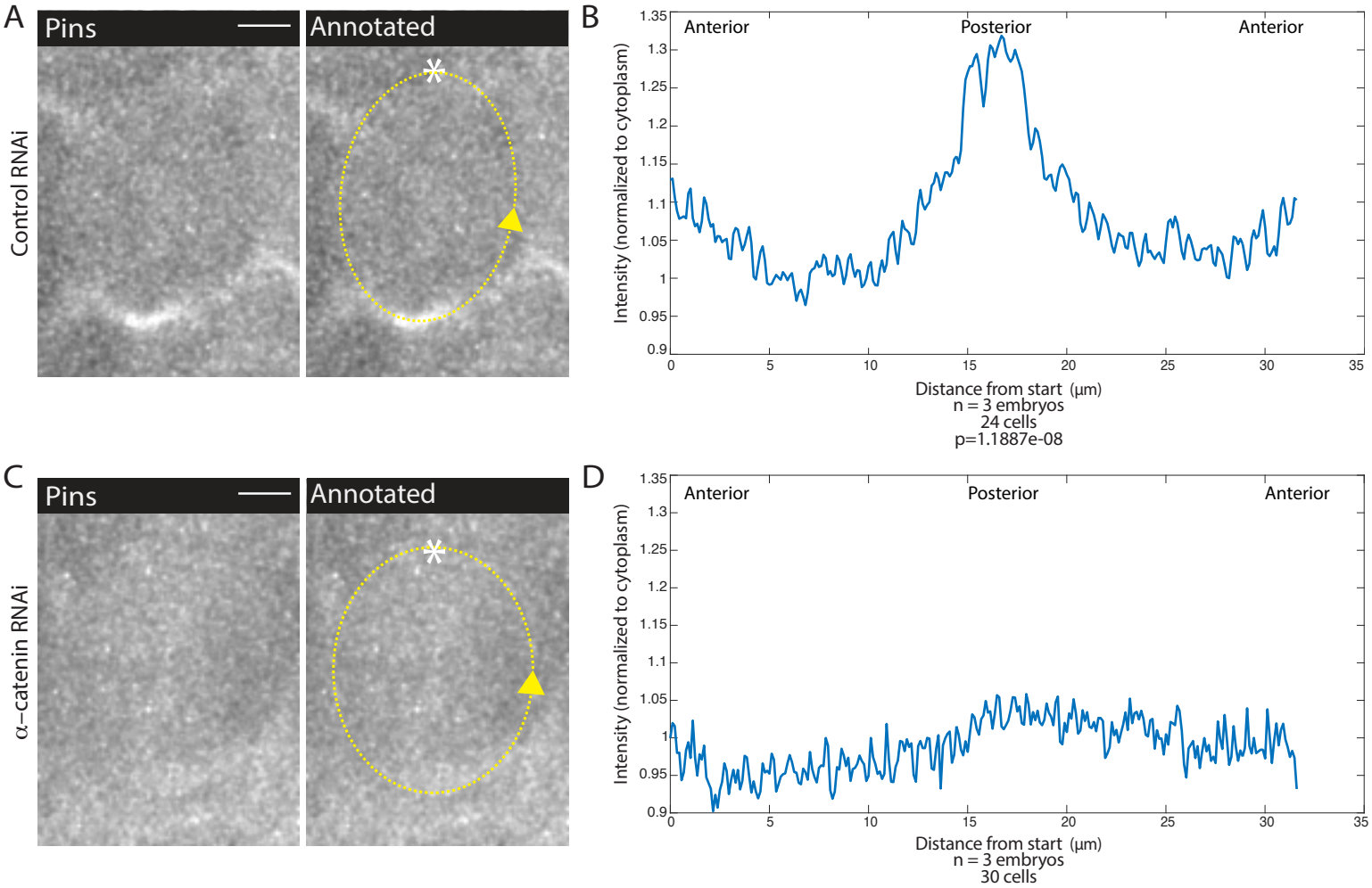
A
Pins
Annotated
Control RNAi
B
Anterior
Posterior
Anterior
Intensity (normalized to cytoplasm)
Distance from start (μm)
n = 3 embryos
24 cells
p=1.1887e-08
C
Pins
Annotated
α−catenin RNAi
D
Anterior
Posterior
Anterior
Intensity (normalized to cytoplasm)
Distance from start (μm)
n = 3 embryos
30 cells

Figure 6. Mechanical force is necessary for Pins polarity and spindle orientation (A, E) Cytoskeletal disruption prevents Pins localization. Image of MD1 in control embryo (A, DMSO injection) or MD1 of cytochalasin D (CytoD) injected embryo (E, 0.25mg/mL CytoD injection). Images show labelled Pins (Pins::YFP), red arrows point to crescents of Pins in control MD1, scalebar is 10 µm. (B, F) Cytoskeletal disruption interferes with division orientation. Image of MD1 of control embryo, same embryo as A, (B, DMSO injection) or MD1 of CytoD injected embryo (F). Images, from same embryo as E, show marker (Tubulin::mCherry) to mark mitotic spindles (greyscale), scalebar is 10 µm. Right, same image annotated with dashed lines to indicate spindle position. (C, G) Quantification of Pins intensity for control embryos (C, DMSO injection) or CytoD injected embryo (G, 0.25mg/mL CytoD injection). Intensity was normalized to cytoplasm. For control (DMSO injection) MD1, n=3 embryos and 30 cells. For CytoD injection MD1, n=3 and 28 cells. (D, H) Quantification of spindle angles for control embryos (H, DMSO injection) or CytoD injected embryo (H) using rose plots. For control embryos (DMSO injection) MD1, n=5 embryos and 162 spindles. For CytoD injection MD1, n=6 embryos and 143 spindles. When compared to control (DMSO injection) using Mann-Whitney, p=0.0043. (I) Schematic of laser ablation schema. The ROI for laser cutting was drawn around MD1 on one side of the embryo to mechanically uncouple MD1 from surrounding tissue. The other side of MD1 was not cut. (J-K) Separating MD1 from surrounding tissue disrupts spindle orientation. Left, image of MD1 on control side of embryo (J, non-cut) or laser cut side of embryo (K). Images show marker (Tubulin::mCherry) to mark mitotic spindles (greyscale), scalebar is 10 µm. Right, same image annotated with dashed lines to indicate spindle position, red box indicates laser cut ROI. (M-N) Quantification of spindle angles for MD1 of control side (M, non-cut), or laser cut side (N) using rose plots. For control side (non-cut) MD1, n=2 embryos and 15 spindles. For laser cut side MD1, n=4 embryos and 56 spindles. Average orientation angles per embryo were statistically different between laser cut embryos and sham ablation embryos, Mann-Whitney, p=0.0286. (O-P) Quantification of spindle angles for DV cut embryos (O) or AP cut embryos (P) using rose plots. For DV cut embryos MD1, n=4 embryos and 91 spindles. Average orientation angles per embryo were not different between DV cut and sham ablated control embryos, Mann-Whitney, p=1. For AP cut embryos MD1, n=4 embryos and 101 spindles. Average orientation angles per embryo were different between AP cut and sham ablated control embryos, Mann-Whitney, p=0.0286.

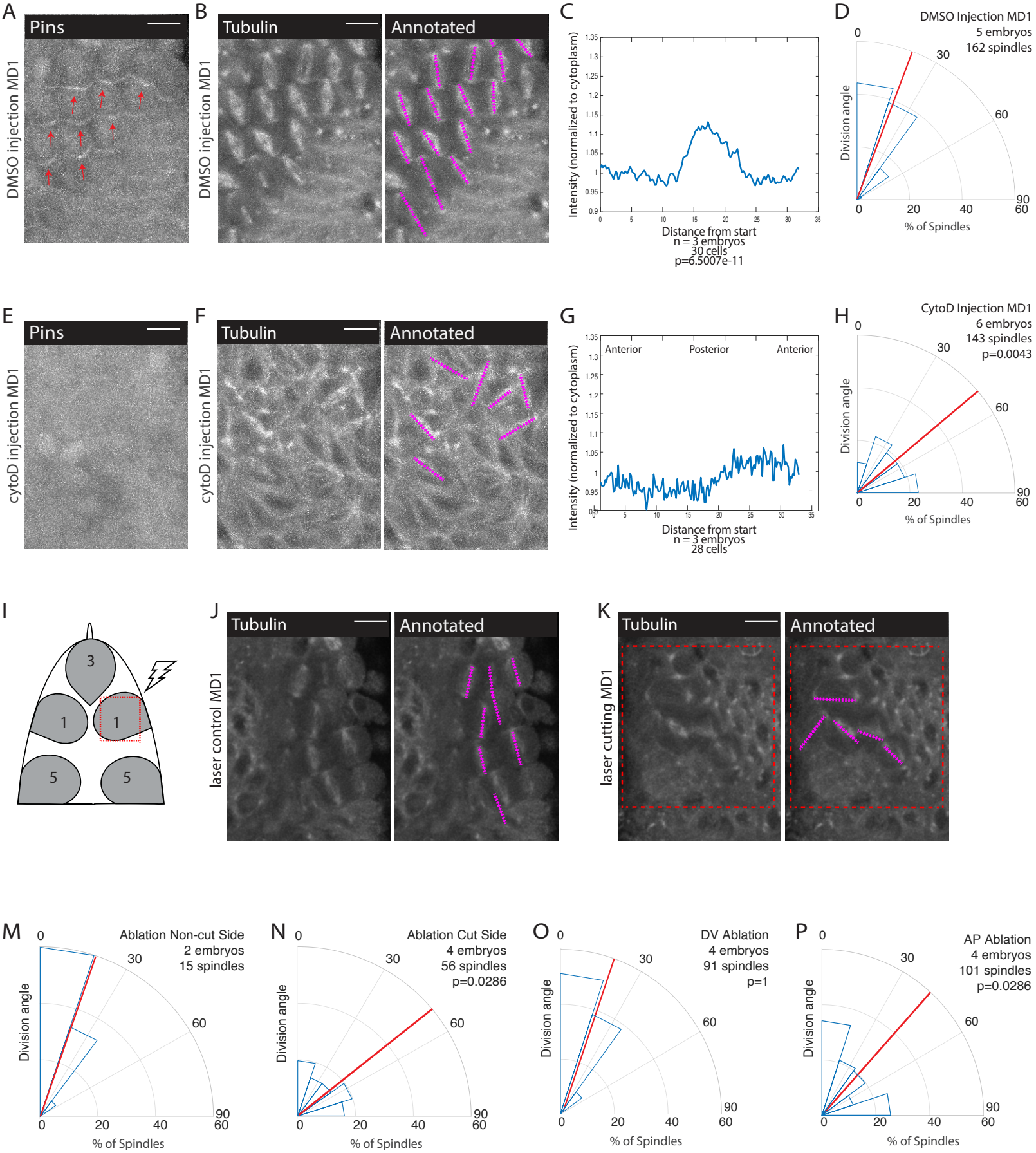
A
Pins
DMSO injection MD1
B
Tubulin
Annotated
DMSO injection MD1
C
Intensity (normalized to cytoplasm)
Distance from start
n = 3 embryos
30 cells
p=6.5007e-11
D
DMSO Injection MD1
5 embryos
162 spindles
Division angle
% of Spindles
E
Pins
cytoD injection MD1
F
Tubulin
Annotated
cytoD injection MD1
G
Anterior
Posterior
Anterior
Intensity (normalized to cytoplasm)
Distance from start
n = 3 embryos
28 cells
H
CytoD Injection MD1
6 embryos
143 spindles
p=0.0043
Division angle
% of Spindles
I
3
1
1
5
5
J
Tubulin
Annotated
laser control MD1
K
Tubulin
Annotated
laser cutting MD1
M
Ablation Non-cut Side
2 embryos
15 spindles
Division angle
% of Spindles
N
Ablation Cut Side
4 embryos
56 spindles
p=0.0286
Division angle
% of Spindles
O
DV Ablation
4 embryos
91 spindles
p=1
Division angle
% of Spindles
P
AP Ablation
4 embryos
101 spindles
p=0.0286
Division angle
% of Spindles

1267 **Figure 7. Snail depletion disrupts Pins polarization and spindle orientation** (A, E) Disrupting
1268 ventral furrow formation disrupts Pins polarity. Image of MD1 of control embryo (A, 0.1x TE buffer
1269 injection) or MD1 of Snail dsRNA injected embryo (E). Images show labelled Pins (Pins::YFP),
1270 red arrows point to crescents of Pins in control, scalebar is 10 µm. (B, F) Snail depletion disrupts
1271 division orientation. Left, image of MD1 of control embryo (B, 0.1x TE buffer injection) or MD1 of
1272 Snail depleted embryo (F). Images show marker (Tubulin::mCherry) to mark mitotic spindles
1273 (greyscale), scalebar is 10 µm. Right, same image annotated with dashed lines to indicate spindle
1274 position. (C, G) Quantification of Pins intensity for control embryos (C, 0.1x TE buffer injection) or
1275 Snail dsRNA injected embryo (G). Intensity was normalized to cytoplasm. For control (0.1x TE
1276 buffer injection) MD1, n=3 embryos and 30 cells. For Snail depletion MD1, n=2 and 20 cells. (D,
1277 H) Quantification of spindle angles for control embryos (H, 0.1x TE buffer injection) or Snail
1278 dsRNA injected embryo (H) using rose plots. For control embryos (0.1x TE buffer injection) MD1,
1279 n=8 embryos and 199 spindles. For Snail dsRNA injection MD1, n=3 embryos and 42 spindles.
1280 Average orientation angles per embryo were statistically different between control and Snail
1281 dsRNA injected embryos, Mann-Whitney, p=0.0121. (I) Schematic summary of laser cutting
1282 experiments. Complete domain isolation results in disrupted division orientation. Isolation from
1283 the ventral furrow through AP cutting also resulted in disrupted division orientation, whereas
1284 isolation from the cephalic furrow through DV cutting did not affect division orientation.

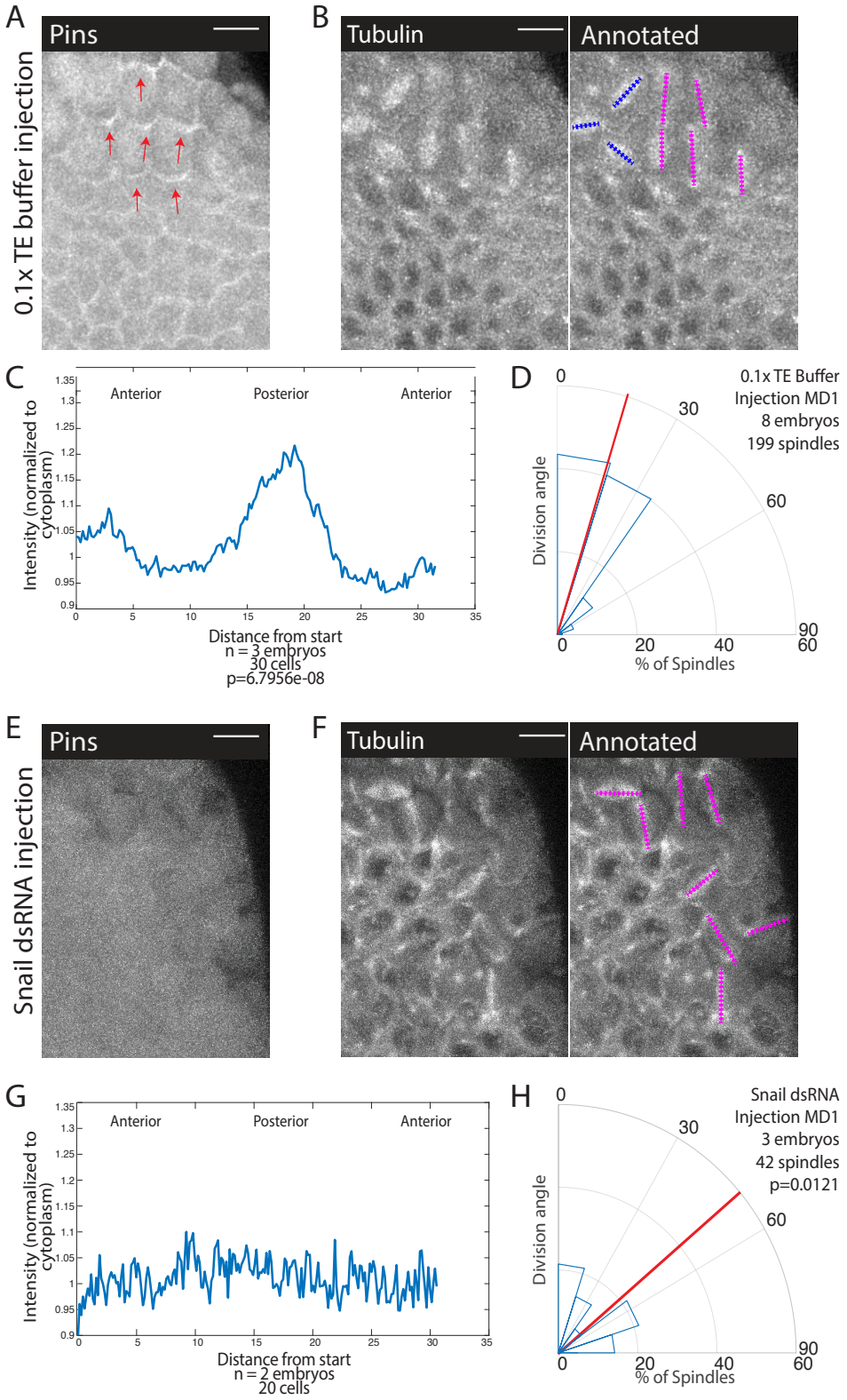
A
Pins
0.1x TE buffer injection
B
Tubulin
Annotated
C
Anterior
Posterior
Anterior
Intensity (normalized to cytoplasm)
Distance from start
n = 3 embryos
30 cells
p=6.7956e-08
D
0.1x TE Buffer
Injection MD1
8 embryos
199 spindles
Division angle
% of Spindles
E
Pins
Snail dsRNA injection
F
Tubulin
Annotated
G
Anterior
Posterior
Anterior
Intensity (normalized to cytoplasm)
Distance from start
n = 2 embryos
20 cells
H
Snail dsRNA
Injection MD1
3 embryos
42 spindles
p=0.0121
Division angle
% of Spindles

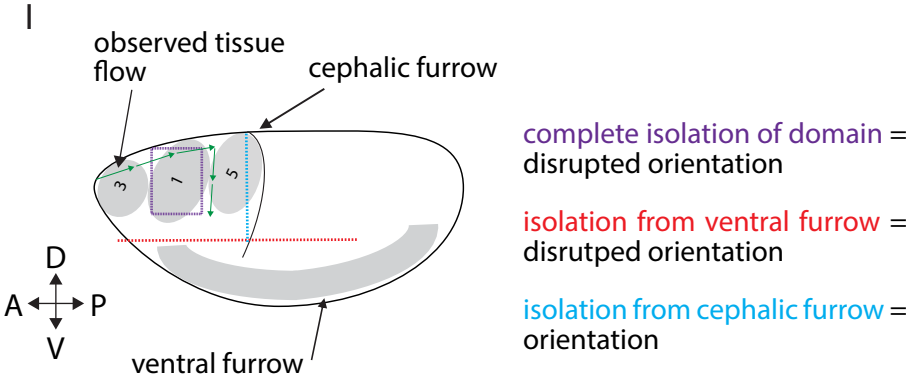
I
observed tissue flow
cephalic furrow
ventral furrow
D
A
P
V
complete isolation of domain = disrupted orientation
isolation from ventral furrow = disrutped orientation
isolation from cephalic furrow = orientation